

# Non-perturbative renormalisation group for the Kardar-Parisi-Zhang equation: general framework and first applications

Léonie Canet<sup>1</sup>, Hugues Chaté<sup>2</sup>, Bertrand Delamotte<sup>3</sup> and Nicolás Wschebor<sup>4</sup>

<sup>1</sup> *Université Joseph Fourier Grenoble I / CNRS UMR 5493,*

*Laboratoire de Physique et Modélisation des Milieux Condensés, BP166, 38042 Grenoble Cedex, France*

<sup>2</sup> *CEA, Service de Physique de l'État Condensé,*

*Centre d'Études de Saclay, 91191 Gif-sur-Yvette, France*

<sup>3</sup> *Laboratoire de Physique Théorique de la Matière Condensée, CNRS UMR 7600,*

*Université Pierre et Marie Curie, 75252 Paris Cedex 05, France*

<sup>4</sup> *Instituto de Física, Facultad de Ingeniería, Universidad de la República, J.H.y Reissig 565, 11000 Montevideo, Uruguay*

We present an analytical method, rooted in the non-perturbative renormalisation group, that allows one to calculate the critical exponents and the correlation and response functions of the Kardar-Parisi-Zhang (KPZ) growth equation in all its different regimes, including the strong-coupling one. We analyze the symmetries of the KPZ problem and derive an approximation scheme that satisfies the linearly realized ones. We implement this scheme at the minimal order in the response field, and show that it yields a complete, qualitatively correct phase diagram in all dimensions, with reasonable values for the critical exponents in physical dimensions. We also compute in one dimension the full (momentum and frequency dependent) correlation function, and the associated universal scaling function. We find good quantitative agreement with the exact result from Praehofer and Spohn [1]. In particular, we obtain, for the universal amplitude ratio,  $g_0 \simeq 1.13(2)$ , to be compared with the exact value  $g_0 = 1.1504\dots$  (the Baik-Rain constant [2]). We emphasize that all these results, which can be systematically improved, are obtained with sole input the bare action and the symmetries, without further assumptions on the existence of scaling or on the form of the scaling function.

PACS numbers: 64.60.Ht, 05.10.Cc, 68.35.Fx, 05.70.Ln, 05.40.-a

## I. INTRODUCTION

In their seminal work [3], Kardar, Parisi and Zhang proposed a stochastic continuum equation to describe surface growth through ballistic deposition which reads

$$\frac{\partial h(t, \vec{x})}{\partial t} = \nu \nabla^2 h(t, \vec{x}) + \frac{\lambda}{2} (\nabla h(t, \vec{x}))^2 + \eta(t, \vec{x}) \quad (1)$$

where  $\eta$  is an uncorrelated white noise of strength  $D$ ,  $\langle \eta(t, \vec{x}) \eta(t', \vec{x}') \rangle = 2D \delta^d(\vec{x} - \vec{x}') \delta(t - t')$ , which models randomness in deposition. The term  $\nu \nabla^2 h(t, \vec{x})$  provides the interface with a smoothening mechanism. The insightful feature of Eq. (1) is to take into account the non-linearity of the growth velocity through the inclusion of the term  $\lambda (\nabla h(t, \vec{x}))^2$  which plays an essential role in the large scale properties of the height profile  $h(t, \vec{x})$ .

The KPZ equation (1) is maybe the simplest nonlinear Langevin equation showing non-trivial behavior [4], and as a consequence it arises in connection with an extremely large class of non-equilibrium or disordered systems [4] such as randomly stirred fluid (Burgers equation) [5], directed polymers in random media [6], dissipative transport [7, 8] or magnetic flux lines in superconductors [9]. The KPZ equation has thus emerged as one of the fundamental theoretical models to investigate universality classes in non-equilibrium scaling phenomena and phase transitions [4]. It is only recently, though, that a definitively-convincing experimental realization has been brought out, confirming detailed theoretical predictions [10].

The profile of the stationary interface is usually char-

acterized by the two-point correlation function

$$C(t, |\vec{x}|) \equiv \langle [h(t, \vec{x}) - h(0, 0) - t \langle \partial_t h \rangle]^2 \rangle \quad (2)$$

and, in particular, by its large scale properties. The KPZ growth leads to generic scaling. At long time  $\tau$  and large distance  $L$ ,  $C$  assumes the scaling form  $C(\tau, L) \propto \tau^{2\chi/z} g(\text{const.} L^{2\chi} \tau^{2\chi/z})$  without fine-tuning any parameter of the model. The scaling function  $g$  is universal and has the asymptotics  $g(y) \rightarrow \text{const.}$  as  $y \rightarrow 0$  and  $g(y) \sim |y|$  as  $y \rightarrow \infty$ .  $\chi$  and  $z$  are the universal roughness and dynamical exponents respectively. In fact, these two exponents are not independent since the Galilean symmetry [5] — the invariance of Eq. (1) under an infinitesimal tilting of the interface — enforces the scaling relation  $z + \chi = 2$  at any non-gaussian fixed-point.

The KPZ equation encompasses two distinct scenarios depending on the dimension of the interface. Above two dimensions, Eq. (1) entails two different regimes, separated by a critical value  $\lambda_c$  of the nonlinear coefficient [3, 5]. In the weak-coupling regime ( $\lambda < \lambda_c$ ), the interface remains smooth, its properties are determined by the  $\lambda = 0$  (gaussian) fixed point — corresponding to the linear Edwards-Wilkinson equation [4] — with exponents  $\chi = (2 - d)/d$  and  $z = 2$ . In the strong-coupling regime ( $\lambda > \lambda_c$ ), the non-linearity becomes relevant and the interface roughens. In this regime, the exponents are not known exactly, and some important issues are still controversial, such as the existence of an upper critical dimension (for a recent discussion, see *e.g.* [11]). This unsatisfactory situation has persisted up to very recently [12] because the strong coupling phase of the KPZ equa-

tion has remained out of reach of controlled analytical approaches. In particular, standard perturbation expansions fail *at all order* to find a strong coupling fixed point [13]. Some non-perturbative approaches have been devised, such as the mode-coupling (MC) approximation [7, 14–17], or the weak noise scheme [18], but they are difficult to improve in practice so that error bars are not easily assessed. (Some specific comments regarding the MC approximation are put forward throughout the paper). Let us finally mention the self-consistent expansion which has yielded some important results (see [19] and references therein).

In two dimensions and below, the situation is different, both from a physical and a theoretical point of view since the interface always roughens. On the theoretical side, exact results are available in one dimension [1, 2, 20–22]. The critical exponents  $\chi = 1/2$  and  $z = 3/2$  have been known for long since they are fixed by the existence of an incidental fluctuation-dissipation theorem [3], but the scaling function  $g(y)$  (and other properties) have been computed exactly only very recently [1, 2, 21, 22]. Note that there had been earlier attempts to determine the scaling function, in the framework of the mode-coupling approximation [14, 23, 24]. In Ref. [24], a refined ansatz for the scaling function is devised to solve self-consistently the MC equations and it turns out that the result compares accurately with the exact solution. The MC is an ‘ad hoc’ approximation which consists in resumming one-loop diagrams while discarding vertex corrections. The quality of the results is all the more surprising that it was shown that the contribution of the neglected terms are of the same order as those kept [14]. The main drawbacks of the MC approach are that it strongly relies on the quality of the ‘educated guess’ for the ansatz and it cannot in practice be systematically improved by calculating higher orders.

Recently, we have proposed an analytical approach to the KPZ equation based on non-perturbative renormalisation group (NPRG) techniques [12]. We showed that a very simple approximation to implement the NPRG yields significant progress since it embeds the strong-coupling fixed-point in all dimensions. It thus provides a complete, qualitatively correct phase diagram in all dimensions, as well as reasonable values for the strong-coupling fixed point exponent in physical dimensions.

Here we present a general and systematic framework, strongly constrained by the symmetries of the problem. We derive general Ward identities and introduce a ‘covariantization’ associated with the Galilean symmetry which, to the best of our knowledge, has never been reported before in the literature. Within this formalism, successive approximations are easily made explicit (although probably difficult to implement at high orders). In the present contribution, we implement the minimal order in the response field of this approximation scheme. We review the (simplified) first account of it presented in [12] – postponing its complete revisited version – and derive new results related to the one-dimensional problem,

in order to confront our approach to the available exact results. In particular, we compute the correlation and scaling functions and show that they are in even better agreement with the exact results of Praehofer and Spohn [1] than those obtained under the MC approximation.

We stress the advantages of the NPRG formalism: (i) it is based on an exact flow equation, which, given a microscopic model, yields the macroscopic properties of the system. The only input is the bare action, that is, no *a priori* knowledge, other than the microscopic model and its symmetries, is required to compute the physical observables. In particular, one does not have to assume scaling at long time and large distance or the form of the scaling function; (ii) the approximations, which are mandatory to solve the exact flow equation can be systematically improved and implemented in any dimension; (iii) beyond scaling, a wealth of quantities can be calculated (for example, we compute here the correction to scaling exponent  $\omega$ ); (iv) it has already yielded many nontrivial and accurate results in systems at equilibrium such as frustrated magnets [25], the random field Ising model [26], membranes [27], bosonic systems [28], but also out-of-equilibrium, where one can mention important advances in reaction-diffusion systems [29].

As the NPRG is a field theoretical method, our starting point is the field theory associated with Eq. (1), which follows from the standard procedure of Janssen-de Dominicis relying in the introduction of a response field  $\tilde{h}$  and sources  $(j, \tilde{j})$  [30]. The generating functional reads:

$$\mathcal{Z}[j, \tilde{j}] = \int \mathcal{D}[h, i\tilde{h}] \exp \left( -S[h, \tilde{h}] + \int_{\mathbf{x}} jh + \tilde{j}\tilde{h} \right) \quad (3)$$

$$S[h, \tilde{h}] = \int_{\mathbf{x}} \left\{ \tilde{h} \left( \partial_t h - \nu \nabla^2 h - \frac{\lambda}{2} (\nabla h)^2 \right) - D \tilde{h}^2 \right\} \quad (4)$$

where  $\mathbf{x} = (t, \vec{x})$ .

The remainder of the paper is organized as follows. In section II, we briefly review the non-perturbative renormalisation group formalism. In section III, we analyze in detail the symmetries of the KPZ action (4) and derive associated Ward identities for the linearly realized ones. In section IV, we build an approximation scheme based on a covariantization procedure rooted in the symmetries, and derive explicitly an *Ansatz* at the minimal order in the response field. The determination of the complete phase diagram in all dimensions and of critical exponents, using a simplified version of this *Ansatz*, is reported in section V. Section VI is then devoted to the calculation, using the full *Ansatz*, of the scaling function and some universal quantities in one dimension, which are then compared with their exact counterparts. Technical details, such as some Ward identities, the computation of vertex functions or the procedures of numerical integration are reported in Appendix A, B and C.

## II. THE NON-PERTURBATIVE RENORMALISATION GROUP

The NPRG formalism relies on Wilson's RG idea, which consists in building a sequence of scale-dependent effective models such that fluctuations are smoothly included as the scale  $\kappa$  is lowered from the microscopic scale  $\Lambda$ , where no fluctuations are taken into account, to the macroscopic one  $\kappa = 0$  where all fluctuations have been summed over [31, 32].

For out-of-equilibrium problems, one formally proceeds as in equilibrium, but handling the presence of response fields and taking care of Itô's discretization and causality properties, as stressed in detail in [33] – which conventions are followed throughout this paper. For future use, we define the Fourier conventions used in [33] and throughout this work:

$$\tilde{f}(\omega, \vec{p}) = \int d^d \vec{x} dt f(t, \vec{x}) e^{i\vec{p} \cdot \vec{x} - i\omega t} \quad (5)$$

$$f(t, \vec{x}) = \int \frac{d^d \vec{p}}{(2\pi)^d} \frac{d\omega}{(2\pi)} \tilde{f}(\omega, \vec{p}) e^{-i\vec{p} \cdot \vec{x} + i\omega t} \quad (6)$$

$$\equiv \int_{\mathbf{p}} \tilde{f}(\mathbf{p}) e^{-i\vec{p} \cdot \vec{x} + i\omega t}, \quad (7)$$

where  $\mathbf{p} = (\omega, \vec{p})$ .

To achieve the separation of modes of the NPRG procedure, one adds to the original action  $\mathcal{S}$ , a momentum-dependent mass-like term:

$$\Delta\mathcal{S}_\kappa = \frac{1}{2} \int_{\mathbf{q}} h_i(\mathbf{q}) [R_\kappa(\mathbf{q})]_{ij} h_j(\mathbf{q}) \quad (8)$$

where the indices  $i, j \in \{1, 2\}$  label the field and response field respectively  $h_1 = h, h_2 = \tilde{h}$ , and summation over repeated indices is implicit. The matrix elements  $[R_\kappa(\mathbf{q})]_{ij}$  are proportional to a cutoff function  $r(q^2/\kappa^2)$  (see section III D), with  $q = \|\vec{q}\|$ , which achieves the selection of fluctuation modes:  $r(x)$  is required to vanish as  $x \gtrsim 1$  such that the fluctuation modes  $h_i(q \gtrsim \kappa)$  are unaffected by  $\Delta\mathcal{S}_\kappa$ , and to be large when  $x \lesssim 1$  such that the other modes ( $h_i(q \lesssim \kappa)$ ) are essentially frozen. Since  $\Delta\mathcal{S}_\kappa$  must preserve the symmetries of the model, we postpone the discussion of the precise structure of the matrix elements  $[R_\kappa(\mathbf{q})]_{ij}$  to section III D after the analysis of these symmetries.

In presence of the mass term  $\Delta\mathcal{S}_\kappa$ , the generating functional (3) becomes scale dependent

$$\mathcal{Z}_\kappa[j, \tilde{j}] = \int \mathcal{D}[h, \tilde{h}] \exp \left( -\mathcal{S} - \Delta\mathcal{S}_\kappa + \int_{\mathbf{x}} j h + \tilde{j} \tilde{h} \right) \quad (9)$$

and the effective action  $\Gamma_\kappa[\varphi, \tilde{\varphi}]$ , where  $\varphi_i = \langle h_i \rangle_{j, \tilde{j}}$  are the expectation values of the fields  $h_i$  in presence of the external sources  $j$  and  $\tilde{j}$ , is given by the Legendre transform of  $\mathcal{W}_\kappa = \log \mathcal{Z}_\kappa$  (up to the term proportional to  $R_\kappa$ ) [31, 33]:

$$\Gamma_\kappa[\varphi, \tilde{\varphi}] + \log \mathcal{Z}_\kappa[j, \tilde{j}] = \int j_i \varphi_i - \frac{1}{2} \int_{\mathbf{q}} \varphi_i [R_\kappa]_{ij} \varphi_j. \quad (10)$$

From  $\Gamma_\kappa$ , one can derive 2-point correlation and response functions,

$$[\Gamma_\kappa^{(2)}]_{i_1 i_2}(\mathbf{x}_1, \mathbf{x}_2, \varphi, \tilde{\varphi}) = \frac{\delta^2 \Gamma_\kappa[\varphi, \tilde{\varphi}]}{\delta \varphi_{i_1}(\mathbf{x}_1) \delta \varphi_{i_2}(\mathbf{x}_2)} \quad (11)$$

and more generally  $n$ -point correlation functions that we write here in a  $2 \times 2$  matrix form (omitting the dependence on the running scale  $\kappa$ )

$$\Gamma_{i_3, \dots, i_n}^{(n)}(\mathbf{x}_1, \dots, \mathbf{x}_n, \varphi, \tilde{\varphi}) = \frac{\delta^{n-2} \Gamma^{(2)}(\mathbf{x}_1, \mathbf{x}_2, \varphi, \tilde{\varphi})}{\delta \varphi_{i_3}(\mathbf{x}_3) \dots \delta \varphi_{i_n}(\mathbf{x}_n)}. \quad (12)$$

The exact flow for  $\Gamma_\kappa[\varphi, \tilde{\varphi}]$  is given by Wetterich's equation which reads (in Fourier space) [31]:

$$\partial_\kappa \Gamma_\kappa = \frac{1}{2} \text{Tr} \int_{\mathbf{q}} \partial_\kappa R_\kappa \cdot G_\kappa \quad \text{with} \quad G_\kappa = [\Gamma_\kappa^{(2)} + R_\kappa]^{-1}. \quad (13)$$

When  $\kappa$  flows from  $\Lambda$  to 0,  $\Gamma_\kappa$  interpolates between the microscopic model  $\Gamma_{\kappa=\Lambda} = \mathcal{S}$  and the full effective action  $\Gamma_{\kappa=0}$  that encompasses all the macroscopic properties of the system [33]. Differentiating Eq. (13) twice with respect to the fields and evaluating it, without prejudice for the following, in uniform and stationary field configurations, one obtains the flow equation for the 2-point functions:

$$\begin{aligned} \partial_\kappa [\Gamma^{(2)}]_{ij}(\mathbf{p}) = & \text{Tr} \int_{\mathbf{q}} \partial_\kappa R(\mathbf{q}) \cdot G(\mathbf{q}) \cdot \left( -\frac{1}{2} \Gamma_{ij}^{(4)}(\mathbf{p}, -\mathbf{p}, \mathbf{q}) \right. \\ & \left. + \Gamma_i^{(3)}(\mathbf{p}, \mathbf{q}) \cdot G(\mathbf{p} + \mathbf{q}) \cdot \Gamma_j^{(3)}(-\mathbf{p}, \mathbf{p} + \mathbf{q}) \right) \cdot G(\mathbf{q}) \end{aligned} \quad (14)$$

where the  $\kappa$  and background fields dependences have been omitted, as well as the last argument of the  $\Gamma^{(n)}$  – with the conventions of Ref. [33], thanks to translational invariance in space and time (as the model is analyzed in the stationary regime).

Solving Eq. (13) (or Eq. (14)) is equivalent to solving the model. This resolution cannot however be exact since, as  $\Gamma_\kappa$  is a functional of the fields  $\varphi(\mathbf{x})$  and  $\tilde{\varphi}(\mathbf{x})$ , Eq. (13) is a non-linear integral partial differential functional equation. Hence one has to devise an approximation scheme. The first constraint on this approximation scheme is to preserve the symmetries of the problem, which we now revisit.

## III. SYMMETRIES OF THE KPZ ACTION

The KPZ action (4) possesses well-known symmetries, in addition to translation and rotation invariances: i) the Galilean symmetry and ii) the  $h$ -shift symmetry, which can be expressed as the invariance of the action (4) under the following transformations:

$$\text{i) } \begin{cases} h'(t, \vec{x}) = \vec{x} \cdot \vec{v} + h(t, \vec{x} + \lambda \vec{v} t) \\ \tilde{h}'(t, \vec{x}) = \tilde{h}(t, \vec{x} + \lambda \vec{v} t). \end{cases} \quad (15)$$

$$\text{ii) } h'(t, \vec{x}) = h(t, \vec{x}) + c \quad (16)$$

where  $\vec{v}$  and  $c$  are arbitrary constant quantities.

In one dimension, the KPZ equation also satisfies a fluctuation-dissipation theorem that fixes the exponents exactly. This relation roots in a time-reversal symmetry of the action which, as shown in [34], corresponds to the transformation

$$\text{iii)} \begin{cases} h'(t, \vec{x}) = -h(-t, \vec{x}) \\ \tilde{h}'(t, \vec{x}) = \tilde{h}(-t, \vec{x}) + \frac{\nu}{D} \nabla^2 h(-t, \vec{x}). \end{cases} \quad (17)$$

One can check that the invariance of the action (4) under this transformation requires that the contribution  $\int \nabla^2 h (\nabla h)^2$  vanishes, which is ‘incidentally’ true only in  $d = 1$ . The time-reversal symmetry thus only holds in that dimension. This set of symmetries entails Ward identities for the  $n$ -point vertex functions, as long as the mass term  $\Delta S_\kappa$  is appropriately chosen (see section IIID).

In fact, there exist even stronger symmetries of the KPZ action that, to our knowledge, were only pointed out in [35]. They consist in ‘gauging’ in time the transformations i) and ii) in the following way:

$$\text{i')} \begin{cases} h'(t, \vec{x}) = \vec{x} \cdot \partial_t \vec{v}(t) + h(t, \vec{x} + \lambda \vec{v}(t)) \\ \tilde{h}'(t, \vec{x}) = \tilde{h}(t, \vec{x} + \lambda \vec{v}(t)) \end{cases} \quad (18)$$

$$\text{ii')} \quad h'(t, \vec{x}) = h(t, \vec{x}) + c(t) \quad (19)$$

which we will refer to as Galilean-gauged and shift-gauged symmetries respectively. Now  $\vec{v}(t)$  and  $c(t)$  are arbitrary infinitesimal functions of time. Note that the action (4) is not strictly invariant under the transformations (18) and (19) but the corresponding variations of the action are linear in the fields, and this behavior also yields useful Ward identities, which we derive in the following. These stronger forms of the symmetries will be thoroughly exploited.

Finally, an additional  $Z_2$  symmetry, which is manifest on the Cole-Hopf version of the theory, is highly nonlinearly realized in the KPZ action (4). The Cole-Hopf field transformation writes:

$$\begin{cases} h(\mathbf{x}) = \frac{2\nu}{\lambda} \log |w(\mathbf{x})| \\ \tilde{h}(\mathbf{x}) = w(\mathbf{x}) \tilde{w}(\mathbf{x}). \end{cases} \quad (20)$$

In terms of  $w$  and  $\tilde{w}$  – upon rescaling these fields and time – the KPZ action becomes:

$$\mathcal{S}[w, \tilde{w}] = \int_{\mathbf{x}} \tilde{w} (\partial_t w - \nabla^2 w) - \frac{1}{4} g_b (w \tilde{w})^2 \quad (21)$$

with the bare coupling constant

$$g_b = \frac{\lambda^2 D}{\nu^3}. \quad (22)$$

This action is invariant under (iv)  $w(t, \vec{x}) \rightarrow \tilde{w}(-t, \vec{x})$ ,  $\tilde{w}(t, \vec{x}) \rightarrow w(-t, \vec{x})$ . Under this symmetry, the fields  $h$

and  $\tilde{h}$  transform as

$$\text{iv)} \begin{cases} h'(t, \vec{x}) = -h(-t, \vec{x}) + \frac{2\nu}{\lambda} \log |\tilde{h}(-t, \vec{x})| \\ \tilde{h}'(t, \vec{x}) = \tilde{h}(-t, \vec{x}). \end{cases} \quad (23)$$

The highly nonlinear character of this  $Z_2$  transformation makes complicated the induced Ward identities among vertex functions, and they are not given here as they are not exploited in the following.

### A. Shift-gauged symmetry

The Ward identity associated with the shift-gauged symmetry can be derived by performing in the functional integral (9) the change of variables corresponding to the transformation (19). As this operation must leave the value of the integral unchanged, one obtains that

$$\int_{\mathbf{x}} \left\{ c(t) j(\mathbf{x}) - \langle \tilde{h}(\mathbf{x}) \rangle_{j, \tilde{j}} \partial_t c(t) - \langle \Delta S_\kappa[c(t), \tilde{h}(\mathbf{x})] \rangle_{j, \tilde{j}} \right\} \quad (24)$$

must vanish, where we have used that  $[R_\kappa(\mathbf{q})]_{11} = 0$  (see Eq. (41)). As the mass term is quadratic in fields,  $\Delta S_\kappa[c(t), \tilde{h}(\mathbf{x})]$  is linear in  $\tilde{h}$ , and thus

$$\langle \Delta S_\kappa[c(t), \tilde{h}(\mathbf{x})] \rangle_{j, \tilde{j}} = \Delta S_\kappa[c(t), \langle \tilde{h}(\mathbf{x}) \rangle] = \tilde{\varphi}(\mathbf{x}).$$

The expression (10) of the Legendre transform then implies

$$\int_{\mathbf{x}} \left\{ c(t) \frac{\delta \Gamma_\kappa[\varphi, \tilde{\varphi}]}{\delta \varphi(\mathbf{x})} - \tilde{\varphi}(\mathbf{x}) \partial_t c(t) \right\} = 0. \quad (25)$$

After integrating by parts the second term, we conclude that the functional

$$\Gamma_\kappa[\varphi, \tilde{\varphi}] - \int_{\mathbf{x}} \tilde{\varphi}(\mathbf{x}) \partial_t \varphi(\mathbf{x}) \quad (26)$$

is invariant under the transformation (19). In other words, the only non-invariant term  $\int \tilde{\varphi} \partial_t \varphi$  of the bare action is not renormalised and the rest of the action is shift-gauged symmetric.

Let us express this property on the  $n$ -point vertex functions, that we write from now on as

$$\Gamma_\kappa^{(l, m)}(\mathbf{x}_1, \dots, \mathbf{x}_{l+m})$$

which stands for the  $\Gamma_\kappa^{(n=l+m)}$  vertex involving  $l$  (resp.  $m$ ) legs – derivatives of  $\Gamma_\kappa$  with respect to  $\varphi$  (resp.  $\tilde{\varphi}$ ) – with the  $l$  first frequencies and momenta referring to the  $\varphi$  fields and the  $m$  last to the  $\tilde{\varphi}$  fields. At this stage, it is convenient to work in Fourier space. The  $n$ -point vertex function are defined in Fourier space by

$$(2\pi)^{d+1}\delta^{d+1}\left(\sum_i \mathbf{p}_i\right)\Gamma_\kappa^{(l,m)}(\mathbf{p}_1,\dots,\mathbf{p}_{l+m-1}) = \int_{\mathbf{x}_1\cdots\mathbf{x}_{l+m}} \Gamma_\kappa^{(l,m)}(\mathbf{x}_1,\dots,\mathbf{x}_{l+m}) e^{i\sum_i (\vec{x}_i\cdot\vec{p}_i - t_i\omega_i)} \quad (27)$$

where again, the last frequency and momentum, fixed by translational invariance in time and space, are implicit. The shift-gauged symmetry entails that the  $n$ -point vertex functions in Fourier space satisfy the following property:

$$\Gamma_\kappa^{(m,n)}(\omega_1, \vec{p}_1 = 0, \dots, \mathbf{p}_{m+n-1}) = i\omega_1\delta_{m1}\delta_{n1} \quad (28)$$

which means that, apart from the contribution of  $\int \tilde{\varphi}\partial_t\varphi$  to  $\Gamma_\kappa^{(1,1)}$ , the vertices vanish upon setting one of the momentum of a  $\varphi$  to zero. This is related to the fact that the field  $\varphi$  only appears in  $\Gamma_\kappa$  with gradients. In particular, it roots the non-renormalisation of the kinetic term of the KPZ action, which is well established in perturbation theory (see *e.g.* [14]).

## B. Galilean symmetry

### 1. Global Galilean symmetry

Let us first review the Ward identities for the standard Galilean symmetry. As for the shift-gauged symmetry, one can prove that, as the transformation (15) corre-

sponding to the Galilean symmetry of the bare action is affine, and as the mass term bears the form (41),  $\Gamma_\kappa$  also possesses this symmetry. The corresponding Ward identity is:

$$\int_{\mathbf{x}} \left\{ (\vec{x}\cdot\vec{v} + \lambda t\vec{v}\cdot\nabla\varphi(\mathbf{x})) \frac{\delta\Gamma_\kappa}{\delta\varphi(\mathbf{x})} + \lambda t\vec{v}\cdot\nabla\tilde{\varphi}(\mathbf{x}) \frac{\delta\Gamma_\kappa}{\delta\tilde{\varphi}(\mathbf{x})} \right\} = 0, \quad (29)$$

that is  $\Gamma_\kappa$  is invariant under the same Galilean symmetry (with the same parameter) as the bare action. One can then proceed to the derivation of the Ward identities for the vertex functions, by taking functional derivatives of Eq. (29) with respect to the fields and then evaluating them for uniform and static fields. For instance, one gets the standard identity for the 3-point function:

$$i\frac{\partial}{\partial\vec{p}}\Gamma_\kappa^{(2,1)}(\omega=0, \vec{p}=\vec{0}; \omega_1, \vec{p}_1) = \lambda\vec{p}_1\frac{\partial}{\partial\omega_1}\Gamma_\kappa^{(1,1)}(\omega_1, \vec{p}_1). \quad (30)$$

The Ward identity for a generic  $n$ -point function can be derived and writes:

$$i\frac{\partial}{\partial\vec{p}}\Gamma_\kappa^{(m+1,n)}(\omega=0, \vec{p}=\vec{0}; \mathbf{p}_1; \dots; \mathbf{p}_{m+n-1}) = \lambda\left(\vec{p}_1\frac{\partial}{\partial\omega_1} + \dots + \vec{p}_{m+n-1}\frac{\partial}{\partial\omega_{m+n-1}}\right)\Gamma_\kappa^{(m,n)}(\mathbf{p}_1; \dots; \mathbf{p}_{m+n-1}). \quad (31)$$

### 2. Galilean-gauged symmetry

Let us now come to the gauged form of the Galilean symmetry (18). As for the shift-gauged symmetry, the variation of the action under this transformation is linear in the fields and consequently, it entails a Ward identity which reads

$$\int d^d\vec{x} \left\{ \lambda\nabla\varphi(\mathbf{x})\frac{\delta\Gamma_\kappa}{\delta\varphi(\mathbf{x})} - \vec{x}\partial_t\frac{\delta\Gamma_\kappa}{\delta\varphi(\mathbf{x})} + \lambda\nabla\tilde{\varphi}(\mathbf{x})\frac{\delta\Gamma_\kappa}{\delta\tilde{\varphi}(\mathbf{x})} - \vec{x}\partial_t^2\tilde{\varphi}(\mathbf{x}) \right\} = 0. \quad (32)$$

From this functional identity, one can again deduce identities for the vertex functions. They bare similar expressions as those for the global Galilean symmetry, but with a stronger content. For instance, the identity for the

three-point function becomes:

$$i\omega\frac{\partial}{\partial\vec{p}}\Gamma_\kappa^{(2,1)}(\omega, \vec{p}=\vec{0}; \omega_1, \vec{p}_1) = \lambda\vec{p}_1 \times \left( \Gamma_\kappa^{(1,1)}(\omega + \omega_1, \vec{p}_1) - \Gamma_\kappa^{(1,1)}(\omega_1, \vec{p}_1) \right), \quad (33)$$

which in the limit  $\omega \rightarrow 0$  coincides with (30). The gauged identity (33) is stronger as it constrains the whole frequency dependence and not only the zero-frequency sector. One could derive similar identities for generic  $n$ -point functions, but we now stress, instead, a more efficient way to exploit the Galilean symmetry, that will guide our construction of the approximation scheme.

### 3. Covariant time derivatives

The previous Ward identities do not clearly reflect the geometrical interpretation of the Galilean symmetry. In order to do so, one can analyse this symmetry from another angle. One can build quantities which are manifestly scalar under the Galilean transformation (15), upon introducing an adequate covariant time derivative. Let us define a function  $f(\mathbf{x})$  as a scalar under the Galilean symmetry if its infinitesimal transform under (15) is given by

$$\delta f(\mathbf{x}) = t\lambda\vec{v} \cdot \nabla f(\mathbf{x}). \quad (34)$$

With this definition, if  $f$  is a scalar,  $\int d^d\vec{x}f$  is invariant under the Galilean transformation and can be used to build an action possessing the Galilean symmetry. It follows from this definition that the response field  $h$  is a scalar, but that the field  $h$  is not unless one takes two successive space derivatives  $\nabla_i \nabla_j h$ . The gradient of a scalar remains a scalar, but not its time derivative since

$$\delta(\partial_t f(\mathbf{x})) = \lambda\vec{v} \cdot (t\nabla(\partial_t f(\mathbf{x})) + \nabla f(\mathbf{x})). \quad (35)$$

As in fluid mechanics, one can construct a covariant time derivative

$$\tilde{D}_t \equiv \partial_t - \lambda\nabla h(\mathbf{x}) \cdot \nabla$$

which conserves the scalar property, *i.e.* if  $f$  is a scalar, so is  $\tilde{D}_t f$ . Note that the covariant derivative of the field  $h$  itself bares a special form *via* a  $1/2$  factor:

$$D_t h(\mathbf{x}) \equiv \partial_t h(\mathbf{x}) - \frac{\lambda}{2}(\nabla h(\mathbf{x}))^2 \quad (36)$$

since  $h$  is not a scalar on its own. The covariant derivatives above constitute the building blocks in the construction of our approximation scheme.

### C. Time-reversal symmetry in $d = 1$

In  $d = 1$ , the action (4) with a mass term of the form (41) has the additional time-reversal symmetry. Note that this is a discrete symmetry (*i.e.* there is no infinitesimal transformation corresponding to (17)). However, as it is linear, one can show using the same procedure as before that  $\Gamma_\kappa$  also possesses this symmetry. That is, it verifies:

$$\Gamma_\kappa[\varphi(\mathbf{x}), \tilde{\varphi}(\mathbf{x})] = \Gamma_\kappa[-\varphi(-t, \vec{x}), \tilde{\varphi}(-t, \vec{x}) + \frac{\nu}{D}\nabla^2\varphi(-t, \vec{x})]. \quad (37)$$

Again, one can derive Ward identities for the  $n$ -point functions by taking derivatives of (37) and evaluating the result at uniform and static fields. For the 2-point functions, this yields, in Fourier space:

$$\begin{aligned} \Gamma_\kappa^{(2,0)}(\omega, \vec{p}) &= \Gamma_\kappa^{(2,0)}(-\omega, \vec{p}) + \frac{\nu}{D}p^2\Gamma_\kappa^{(1,1)}(-\omega, \vec{p}) \\ &+ \frac{\nu}{D}p^2\Gamma_\kappa^{(1,1)}(\omega, -\vec{p}) + \left(\frac{\nu}{D}\right)^2 p^4\Gamma_\kappa^{(0,2)}(-\omega, \vec{p}). \end{aligned} \quad (38)$$

which, given that  $\Gamma_\kappa^{(2,0)}(\omega, \vec{p}) = \Gamma_\kappa^{(2,0)}(-\omega, \vec{p})$  and spatial parity reduces to:

$$2\text{Re}\Gamma_\kappa^{(1,1)}(\mathbf{p}) = -\frac{\nu}{D}p^2\Gamma_\kappa^{(0,2)}(\mathbf{p}). \quad (39)$$

For the 3-point functions, one gets:

$$\begin{aligned} 2\text{Re}\Gamma_\kappa^{(1,2)}(\mathbf{p}_1; \mathbf{p}_2) &= -\frac{\nu}{D}p_1^2\Gamma_\kappa^{(0,3)}(\mathbf{p}_1; \mathbf{p}_2). \\ 2\text{Im}\Gamma_\kappa^{(2,1)}(\mathbf{p}_1; \mathbf{p}_2) &= -\frac{\nu}{D}p_2^2\text{Im}\Gamma_\kappa^{(1,2)}(\mathbf{p}_1; \mathbf{p}_2) \\ &\quad -\frac{\nu}{D}p_1^2\text{Im}\Gamma_\kappa^{(1,2)}(\mathbf{p}_2; \mathbf{p}_1). \end{aligned} \quad (40)$$

Similar expressions can be derived for  $\Gamma_\kappa^{(3,0)}$  and the 4-point functions, which are reported for completeness in Appendix A.

### D. Cut-off function

The mass term  $\Delta\mathcal{S}_\kappa$  defined by (8) must be chosen such that the Ward identities are preserved along the flow. This is not obvious *a priori*. In particular, a quadratic mass term cannot be invariant under the shift-gauged symmetry. However, as explained above, if the variation of  $\Delta\mathcal{S}_\kappa$  under the transformation (19) is linear in the field, the Ward identity remains identical even in the presence of such a term. Similar comments hold for the Galilean symmetry, which is preserved as long as the cut-off matrix  $R_\kappa$  does not depend on the frequency. We thus choose a frequency independent matrix  $R_\kappa$  – which also preserves causality properties [33]. Moreover, the time-reversal symmetry imposes the following relation between its components:  $[R_\kappa(\vec{q})]_{12} = -\frac{\nu}{2D}q^2 [R_\kappa(\vec{q})]_{22}$ , which we will impose in all dimensions.

Finally, we take  $[R_\kappa(\vec{q})]_{11} = 0$  since it is not necessary to consider a cutoff term proportional to  $\varphi\varphi$  and since the presence of such a term would spoil the property that  $\Gamma_\kappa$  is proportional to  $\tilde{\varphi}$ , see [33].

Consequently, the cutoff matrix has the following form:

$$R_\kappa(\vec{q}) = r \begin{pmatrix} \frac{q^2}{\kappa^2} & 0 \\ \nu_\kappa q^2 & -2D_\kappa \end{pmatrix}, \quad (41)$$

where the running coefficients  $\nu_\kappa$  and  $D_\kappa$  are introduced for convenience [12]. Here we use  $r(x) = \alpha/(\exp(x) - 1)$  where  $\alpha$  is a free parameter.

## IV. APPROXIMATION SCHEME

Two routes have been followed in the past to build approximation schemes to deal with exact NPRG flow equations. Either one focusses on the long-time and large-distance properties, trying to describe as accurately as possible the zero-momentum and zero-frequency domain while approximating the other sectors. Or the aim is to compute the momentum and frequency dependence of

two-point functions and then the approximation is performed on the three and four point functions.

The usual implementation of the first route consists in performing a ‘derivative expansion’:  $\Gamma_\kappa$  is expanded in powers of gradients and time derivatives of the fields [31, 33]. This strategy has been undertaken to investigate the critical properties of many equilibrium [31], and also non-equilibrium systems such as reaction-diffusion processes [29], where it has yielded satisfactory results. However, for the KPZ problem, the signature nonlinear term involves a gradient, and this seems to preclude the use of the derivative expansion [34].

The second route is the one followed here. At equilibrium, one can compute the momentum dependence of the two-point function using the Blaizot-Méndez-Wschebor (BMW) approximation scheme which has proved to yield very accurate results for  $O(N)$  models [36]. In the BMW framework, the momentum dependence of  $\Gamma_\kappa^{(3)}$  and  $\Gamma_\kappa^{(4)}$  in the flow equation for  $\Gamma_\kappa^{(2)}$  is truncated. However, a direct implementation of the BMW method for the KPZ problem is hindered by the symmetries which impose strict identities between  $\Gamma_\kappa^{(m,n)}$ ’s with different  $m$  and at different momenta, see *e.g.* Eq. (31).

To overcome this difficulty, we propose instead to construct an *Ansatz* for  $\Gamma_\kappa$  that manifestly preserves the shift-gauged and Galilean-gauged symmetries while allowing for arbitrary frequency and momentum dependences in the two-point functions. This is easily achieved by combining together the basic Galilean scalars of the theory –  $\tilde{\varphi}$ ,  $\nabla_i \nabla_j \varphi$  and  $D_t \varphi$ , and their gradients and covariant derivatives  $\tilde{D}_t$  – since, by construction, all calculations involving a functional of these quantities automatically satisfy the Galilean symmetry (the other symmetries, but the nonlinearly realized one, being easily enforced afterwards).

On this basis, various truncations may be performed. One could, for example, keep complete dependences in  $\tilde{\varphi}$  and  $\nabla^2 \varphi$ , while treating only the zero-frequency sector. This ‘super derivative expansion’ option is left for future studies. An alternative choice, pursued here, is to

keep a complete dependence in both momentum and frequency of the two-point functions, while truncating its field dependence. Note that the truncations in  $\varphi$  or  $\tilde{\varphi}$  are not equivalent at a given order since the dependence in  $\varphi$ , contrary to that in  $\tilde{\varphi}$ , is highly constrained by the Galilean symmetry.

In the following, with the ultimate aim of confronting the obtained correlation and scaling functions in one dimension with the exact ones, we build an *Ansatz* for  $\Gamma_\kappa$  with a minimal field dependence. This amounts to keep terms at most quadratic in  $\tilde{\varphi}$  and linear in  $\nabla^2 \varphi$  and in  $D_t \varphi$ , but to combine them with arbitrary powers of gradients  $\nabla^2$  and covariant time derivatives  $\tilde{D}_t$  to allow for an arbitrary dependence in momentum and frequency. Consequently, the dependence in  $\varphi$  is not restricted to be polynomial since arbitrary powers of this field are included through the covariant derivative  $\tilde{D}_t$ .

The BMW method can accurately capture the momentum dependence of two-point functions [36]. We can therefore be confident *a priori* that the approximation scheme outlined above, which is close in spirit to the BMW approximation – the difference residing in terms subleading from the BMW point of view which are here included so as to preserve the Galilean symmetry, should be sufficient to get a reliable description of the frequency and momentum dependence of two-point functions. There is, however, a specificity inherent to the KPZ problem. The Galilean symmetry prevents the regulator from depending on frequencies (see section III D). This renders an expansion in internal frequencies (as would suggest the BMW scheme) unjustified. This difficulty is hopefully circumvented by the fact that if vertices are expanded in momenta, then the Galilean-gauged symmetry fixes the frequency dependence associated with  $\phi$ -legs (see *e.g.* Eq. (33)). Accordingly, no frequency expansion is needed for the  $\phi$ -legs.

The main source of inaccuracy of the present scheme probably lies in the field expansion and in particular in the  $\tilde{\varphi}$  truncation [37]. We leave for future work this study. To summarize all the previous discussions, the *Ansatz* considered in the following thus writes:

$$\Gamma_\kappa[\varphi, \tilde{\varphi}] = \int_{\mathbf{x}} \left\{ \tilde{\varphi} f_\kappa^\lambda(-\tilde{D}_t^2, -\nabla^2) D_t \varphi - \tilde{\varphi} f_\kappa^D(-\tilde{D}_t^2, -\nabla^2) \tilde{\varphi} - \frac{\nu}{2D} \left[ \nabla^2 \varphi f_\kappa^\nu(-\tilde{D}_t^2, -\nabla^2) \tilde{\varphi} + \tilde{\varphi} f_\kappa^\nu(-\tilde{D}_t^2, -\nabla^2) \nabla^2 \varphi \right] \right\}. \quad (42)$$

The operator  $\tilde{D}_t$  is squared in  $f_\kappa^D$  since this function is real. For  $f_\kappa^\nu$  and  $f_\kappa^\lambda$ , to take the square of  $\tilde{D}_t$  is a choice that ensures a natural separation between real and imaginary parts of  $\Gamma_\kappa^{(1,1)}$ , without loss of generality for the 2-point functions. Note that one needs to make precise the meaning of the expressions  $f_\kappa^X(-\tilde{D}_t^2, -\nabla^2)$  ( $X = D, \nu, \lambda$ ). Indeed, it is ambiguous as it stands since the  $\tilde{D}_t$  and  $\nabla$  operators do not commute. We take the convention that all  $\tilde{D}_t$ ’s are on the left of the  $\nabla$ ’s. We also

assume that these functions can be expanded in series of their arguments:

$$f_\kappa^X(-\tilde{D}_t^2, -\nabla^2) = \sum_{m,n=0}^{\infty} a_{mn} (-\tilde{D}_t^2)^m (-\nabla^2)^n. \quad (43)$$

One can then consider the constraints stemming from the other symmetries. The shift-gauged symmetry imposes that  $f_\kappa^\lambda(\omega^2, \vec{p}^2 = 0) \equiv 1$ . In dimension one, the time-reversal symmetry implies that the two functions

$f_\kappa^D$  et  $f_\kappa^\nu$  become identical, and also that  $f_\kappa^\lambda(\omega^2, \vec{p}^2) \equiv 1$ . In a generic dimension  $d$ , the *Ansatz* (42) thus consists in three independent running functions of  $p^2$  and  $\omega^2$ , and is reduced to a unique function of  $p^2$  and  $\omega^2$  in  $d = 1$ .

To compute the flow equations of the functions  $f_\kappa^X(-\tilde{D}_t^2, -\nabla^2)$ ,  $X = \lambda, \nu$  or  $D$ , one needs the expressions of the  $n$ -point functions up to  $n = 4$ . All the calculations are performed at vanishing fields. For the two-point functions, they are straightforward and yield

$$\begin{aligned}\Gamma_\kappa^{(2,0)}(\omega, \vec{p}) &= 0 \\ \Gamma_\kappa^{(1,1)}(\omega, \vec{p}) &= i\omega f_\kappa^\lambda(\omega^2, \vec{p}^2) + \frac{\nu}{D} \vec{p}^2 f_\kappa^\nu(\omega^2, \vec{p}^2) \\ \Gamma_\kappa^{(0,2)}(\omega, \vec{p}) &= -2f_\kappa^D(\omega^2, \vec{p}^2).\end{aligned}\quad (44)$$

In this case, there is no ambiguity from the ordering of the gradient and covariant time derivative operators. The calculation and the explicit expressions of the 3- and 4-point functions, more lengthy, are detailed in Appendix B. One can check that all the Ward identities derived in section III are satisfied by these functions.

## V. SIMPLIFIED APPROXIMATION

As a first step, the *Ansatz* (42) can be further simplified by constraining the form of the functions  $f_\kappa^X(-\tilde{D}_t^2, -\nabla^2)$ . The idea is to focus on a reliable description of the zero-frequency and momentum sector of the theory while circumventing the limitations of the derivative expansion which is problematic here. For this, one can neglect all  $\tilde{D}_t^2$  dependence in these functions:  $f_\kappa^X(-\tilde{D}_t^2, -\nabla^2) \rightarrow f_\kappa^X(-\nabla^2)$  for  $X = \lambda, \nu$  and  $D$ .

The *Ansatz* proposed in [12], is actually slightly simpler, since we imposed the one-dimensional constraint  $f_\kappa^\lambda = 1$  in *all* dimensions (or stated otherwise we extended the condition  $f_\kappa^\lambda(\vec{p} = 0) = 1$  holding for all  $d$  to the whole  $\vec{p}$  sector). It reads

$$\Gamma_\kappa[\varphi, \tilde{\varphi}] = \int_{\mathbf{x}} \left\{ \tilde{\varphi}(\mathbf{x}) D_t \varphi(\mathbf{x}) - \tilde{\varphi}(\mathbf{x}) f_\kappa^D(-\nabla^2) \tilde{\varphi}(\mathbf{x}) - \frac{\nu}{D} \tilde{\varphi}(\mathbf{x}) f_\kappa^\nu(-\nabla^2) \nabla^2 \varphi(\mathbf{x}) \right\}. \quad (45)$$

As a matter of fact, this *Ansatz* implies that all interaction vertices ( $\Gamma_\kappa^{(n)}$  with  $n > 2$ ) bear their bare form. Among those, the only non-zero one is  $\Gamma_\kappa^{(2,1)}$ :

$$\Gamma_\kappa^{(2,1)}(\omega_1, \vec{p}_1, \omega_2, \vec{p}_2) = \lambda \vec{p}_1 \cdot \vec{p}_2. \quad (46)$$

With the *Ansatz* (45), the 2-point functions in generic dimensions reduce to

$$\begin{aligned}\Gamma_\kappa^{(2,0)}(\omega, \vec{p}) &= 0 \\ \Gamma_\kappa^{(1,1)}(\omega, \vec{p}) &= i\omega + \frac{\nu}{D} \vec{p}^2 f_\kappa^\nu(p^2) \\ \Gamma_\kappa^{(0,2)}(\omega, \vec{p}) &= -2f_\kappa^D(p^2).\end{aligned}\quad (47)$$

The flow equations for the functions  $f_\kappa^\nu$  and  $f_\kappa^D$  and the definition of the critical exponents can be found in [12].

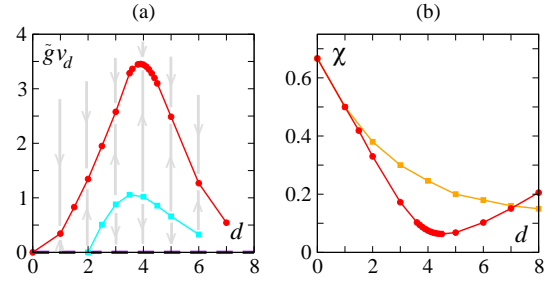


FIG. 1. (Color online) (a) Flow diagram within our approximation in the  $(d, \hat{g}v_d)$  plane (with  $v_d^{-1} = 2^{d+1}\pi^{d/2}\Gamma[\frac{d}{2}]$  a normalization factor related to the integration volume). Red circles: renormalized value  $\hat{g}_{\text{SC}}^*$  at  $F_{\text{SC}}$ . Dashed purple line: Gaussian fixed point  $F_{\text{EW}}$ . Cyan squares: bare value  $\hat{g}_c$ , which separates the basins of attraction of  $F_{\text{SC}}$  and  $F_{\text{EW}}$ . Grey arrows symbolize flow lines. (b) Variation with  $d$  of  $\chi = 2 - z$  for  $F_{\text{SC}}$  (red circles: our results; orange squares: numerical values from [38, 39]. See also Table I.)

TABLE I. Exponent values in integer dimensions. The average numerical values are extracted from [38]. To our knowledge, no estimates of  $\omega$  are available in the literature.

$d$	1	2	3	4
$\chi$ [33]	0.50	0.33	0.17	0.075
$\chi$ (numerics)	0.50	0.38	0.30	0.24
$\omega$ [33]	0.817	0.70	0.63	0.54

Despite its simplicity, this *Ansatz* already gives satisfactory results [12] as it embeds a strong coupling fixed point in all dimensions. It thus yields a complete flow diagram (Fig. 1(a)), and reasonable exponent values in physical dimensions (Fig. 1(b)).

More precisely, in all dimensions studied (*i.e.* up to  $d = 8$ ), the *Ansatz* encompasses, besides the Edwards-Wilkinson fixed point  $F_{\text{EW}}$ , a fully-attractive non-trivial fixed point  $F_{\text{SC}}$ . In all  $d$ , generic scaling is evidenced, *i.e.* the flow always reaches one of these fixed points. For  $d < 2$ ,  $F_{\text{SC}}$  is reached from any initial condition. For  $d > 2$ ,  $F_{\text{EW}}$  becomes locally fully attractive, and there exists a critical bare value  $\hat{g}_c$  (see (22) for the definition of  $g$ ) leading to the roughening transition fixed point  $F_{\text{RT}}$ , which separates the basins of attraction of  $F_{\text{SC}}$  and  $F_{\text{EW}}$ . In  $d = 2$ ,  $F_{\text{RT}}$  coincides with  $F_{\text{EW}}$ , and becomes non-Gaussian for larger dimensions.

Because of the Galilean symmetry and because the coupling constant  $\hat{g}_{\text{SC}}^*$  is non zero,  $F_{\text{SC}}$  is characterized by a single exponent. We thus only discuss below the values obtained for  $\chi$  [12]. Table I and Fig. 1(b) contain our estimates for  $\chi$  and  $\omega$ , the subleading exponent governing the corrections to scaling. For  $d \lesssim 4$ ,  $\chi$  decreases almost linearly with  $d$ , with the exact value  $\frac{1}{2}$  (resp.  $\frac{2}{3}$ ) recovered in  $d = 1$  (resp.  $d = 0$ ), and a reasonable but deteriorating agreement with numerical values for  $2 \leq d \leq 4$ . In higher dimensions,  $\chi$  increases with  $d$ , at odds with both numerical values and the scenario of



$d = 4$  being an upper critical dimension beyond which  $\chi = 0$  [17, 18, 40]. Regarding  $F_{\text{RT}}$ , we record negative values of  $\chi$  for  $2 < d < 5$ , which is reminiscent of perturbative results performed at fixed  $d$  [41] but in contradiction with exact results dictating  $\chi = 0$  [13, 42]. This is to be imputed to our breaking of the  $Z_2$  symmetry manifest in the Cole-Hopf formulation and non-linearly realized in the KPZ problem.

## VI. ONE DIMENSIONAL SCALING FUNCTION

We now consider the full *Ansatz* (42) and calculate the momentum- and frequency-dependent two-point correlation function of the one dimensional problem to extract from it the universal scaling function. We recall that, due to the time-reversal symmetry, the *Ansatz* (42) simplifies in  $d = 1$  since there is only one running function left:  $f_\kappa^D = f_\kappa^\nu \equiv f_\kappa$  and  $f_\kappa^\lambda \equiv 1$ . We also drop from now on the vector arrows and set  $\nu = D = 1$  since these two

coefficients can be absorbed in the action (4) through an appropriate rescaling of the fields and of time and the change of coupling constant  $\lambda \rightarrow \sqrt{g_b} = \lambda D^{1/2}/\nu^{3/2}$ .

### A. Flow equations

The flow equation for the function  $f_\kappa$  can be derived either from the flow of  $\Gamma_\kappa^{(0,2)}$  or from the one of  $\Gamma_\kappa^{(1,1)}$  according to (44). These two flows are equal in  $d = 1$  since the *Ansatz* preserves all the symmetries. They can be computed using Eq. (14), with the propagator matrix  $G_\kappa$  given by

$$G_\kappa(\omega, q) = \frac{1}{P_\kappa(\omega^2, q^2)} \begin{pmatrix} 2k_\kappa(\omega^2, q^2) & Y_\kappa(\omega, q) \\ Y_\kappa^*(\omega, q) & 0 \end{pmatrix} \quad (48)$$

where  $k_\kappa(\omega^2, q^2) = f_\kappa(\omega^2, q^2) + r(q^2/\kappa^2)$ ,  $Y_\kappa(\omega, q) = i\omega + q^2 k_\kappa(\omega^2, q^2)$  and  $P_\kappa(\omega^2, q^2) = \omega^2 + (q^2 k_\kappa)^2$ . The calculation is straightforward and yields:

$$\begin{aligned} \partial_\kappa f_\kappa(\varpi, p) = & -\frac{1}{2} \int_{\mathbf{q}} \partial_\kappa S_\kappa(q) \left\{ \frac{1}{P_\kappa(\omega^2, q^2)} X_\kappa(\omega^2, q^2) \Gamma_\kappa^{(2,2)}(\mathbf{q}, -\mathbf{q}, \mathbf{p}) + \frac{1}{2P_\kappa^2(\omega^2, q^2) P_\kappa((\varpi + \omega)^2, (p + q)^2)} \right. \\ & \times \left[ 2X_\kappa(\omega^2, q^2) Y_\kappa(\varpi + \omega, p + q) \Gamma_\kappa^{(1,2)}(-\mathbf{q}, -\mathbf{p}) \Gamma_\kappa^{(2,1)}(\mathbf{q}, -\mathbf{p} - \mathbf{q}) - q^2 Y_\kappa^2(\omega, q) \Gamma_\kappa^{(1,2)}(-\mathbf{p} - \mathbf{q}, \mathbf{p}) \right. \\ & \times \left( Y_\kappa(\varpi + \omega, p + q) \Gamma_\kappa^{(1,2)}(-\mathbf{q}, -\mathbf{p}) + 2k_\kappa((\varpi + \omega)^2, (p + q)^2) \Gamma_\kappa^{(2,1)}(\mathbf{p} + \mathbf{q}, -\mathbf{q}) \right) \\ & - \left( Y_\kappa^*(\varpi + \omega, p + q) \Gamma_\kappa^{(1,2)}(\mathbf{q}, \mathbf{p}) + 2k_\kappa((\varpi + \omega)^2, (p + q)^2) \Gamma_\kappa^{(2,1)}(\mathbf{q}, -\mathbf{p} - \mathbf{q}) \right) \\ & \left. \times \left( q^2 (Y_\kappa^*)^2(\omega, q) \Gamma_\kappa^{(1,2)}(\mathbf{p} + \mathbf{q}, -\mathbf{p}) - 2X_\kappa(\omega^2, q^2) \Gamma_\kappa^{(2,1)}(\mathbf{p} + \mathbf{q}, -\mathbf{q}) \right) \right\} \quad (49) \end{aligned}$$

where  $\mathbf{q} \equiv (\omega, q)$ ,  $\mathbf{p} \equiv (\varpi, p)$ ,  $X_\kappa(\omega^2, q^2) = \omega^2 - q^4 k_\kappa^2(\omega^2, q^2)$ ,  $S_\kappa(q) = D_\kappa r(q^2/\kappa^2)$  and where the expressions for the 3- and 4-point vertex functions  $\Gamma_\kappa^{(n,m)}$  are given in Appendix B. The flow equation for  $f_\kappa$  is hence an integral over the internal momentum  $q$  and frequency  $\omega$  and depends on the external momentum  $p$  and frequency  $\varpi$ .

As we want to study the fixed point properties, we introduce dimensionless and renormalized quantities. Momenta are measured in units of  $\kappa$ , *e.g.*  $\hat{p} = p/\kappa$ , and frequencies in units of  $D_\kappa \kappa^2$ , *e.g.*  $\hat{\varpi} = \varpi/(D_\kappa \kappa^2)$ . At the bare level,  $f_{\kappa=\Lambda} = D = 1$ , we thus define the dimensionless renormalized function  $\hat{f}_\kappa = f_\kappa/D_\kappa$ . The sole running anomalous dimension  $\eta_\kappa$  is defined by  $\kappa \partial_\kappa \ln D_\kappa = -\eta_\kappa$  so that  $D_\kappa \sim \kappa^{-\eta^*}$  at the fixed point. The scaling exponents in  $d = 1$  are then given by  $z = 2 - \eta^*$  and  $\chi = \eta^*$ . The absolute normalization of  $\hat{f}_\kappa$  and  $D_\kappa$  is fixed by setting  $\hat{f}_\kappa(0, 0) = 1$  – for simplicity and since without much influence on the result [36].

The flow equation for the dimensionless function reads:

$$\begin{aligned} \partial_s \hat{f}_\kappa(\hat{\varpi}, \hat{p}) = & \eta_\kappa \hat{f}_\kappa(\hat{\varpi}, \hat{p}) + (2 - \eta_\kappa) \hat{\varpi} \partial_{\hat{\varpi}} \hat{f}_\kappa(\hat{\varpi}, \hat{p}) \\ & + \hat{p} \partial_{\hat{p}} \hat{f}_\kappa(\hat{\varpi}, \hat{p}) + \frac{1}{D_\kappa} \kappa \partial_\kappa f_\kappa(\varpi, p) \quad (50) \end{aligned}$$

where  $\partial_s = \kappa \partial_\kappa$ . Once the substitutions for dimensionless quantities have been performed in (49), the last term  $\frac{1}{D_\kappa} \partial_\kappa f_\kappa$  is dimensionless, and depends on the external dimensionless momentum  $\hat{p}$  and frequency  $\hat{\varpi}$ .

The dimensionless running coupling constant is in one dimension  $\hat{g}_\kappa = \kappa^{-1} \lambda^2 / D_\kappa^2$ . Its flow equation is reduced to its dimensional part due to Galilean invariance:

$$\partial_s \hat{g}_\kappa = \hat{g}_\kappa (2\eta_\kappa - 1), \quad (51)$$

and one finds as expected that  $\chi = \eta^* = \frac{1}{2}$  at any fixed point with  $\hat{g}^* \neq 0$ .

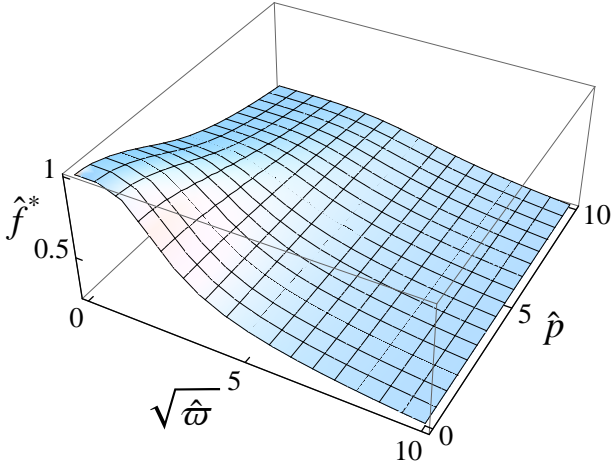


FIG. 2. (Color online) Typical shape of the dimensionless fixed point function  $\hat{f}^*(\hat{\omega}, \hat{p})$  (recorded at  $s = -25$  and for  $\alpha = 1$ ).

### B. Numerical integration

The numerical integration of Eqs. (50) and (51) was performed using standard techniques and the numerical accuracy of the results was checked by using several system sizes, resolutions, *etc.* (see Appendix C). The error inherent to the order of the approximation was estimated by varying the parameter  $\alpha$  of the cut-off function. Indeed, although physical quantities are obtained from the exact NPRG equations (13) and (14) in the limit  $\kappa \rightarrow 0$  and thus do not depend on the choice of the particular profile of  $R_\kappa$ , any approximation introduces a spurious residual dependence on the regulator [43]. Here,  $\alpha$  was varied between 0.5 and 10, only to observe an overall variation of a few percent of all physical quantities. The error bars given below reflect the dispersion stemming from both sources of error.

Runs were started from various different initial conditions including the bare action ( $\hat{f}_\Lambda \equiv 1$ ) with  $\hat{g}$  typically between 1 and 10. In all cases, the function  $\hat{f}_\kappa$  smoothly deformed from its initial shape to eventually reach a fixed point where it stopped evolving, typically after  $s \gtrsim -20$ . In other words, our KPZ flow equations show generic scaling. Fig. 2 shows a typical shape of the fixed point function  $\hat{f}^*(\hat{\omega}, \hat{p})$ . It is fixed by the normalisation condition to unity at vanishing momentum and frequency and decays as a power law when  $\hat{\omega}$  or/and  $\hat{p}$  become large.

### C. Scaling function

#### 1. Extraction of the scaling function

We now turn to the description of the fully attractive fixed point. At this fixed point  $\partial_s \hat{f}_\kappa(\hat{\omega}, \hat{p}) = 0$  (in Eq. (50)) and  $g^* \neq 0$  such that  $\eta_\kappa \equiv \eta^* = \frac{1}{2}$ . Moreover, we

verified numerically that the non-linear term  $\partial_s f_\kappa / D_\kappa$  in (50) decouples (that is  $\partial_s f_\kappa / D_\kappa \rightarrow 0$ ) when  $\hat{\omega} \gg 1$  or/and  $\hat{p} \gg 1$ . As a consequence, at the fixed point, Eq. (50) reduces in this regime to the homogeneous equation

$$\frac{1}{2} \hat{f}_\kappa(\hat{\omega}, \hat{p}) + \hat{p} \partial_{\hat{p}} \hat{f}_\kappa(\hat{\omega}, \hat{p}) + \frac{3}{2} \hat{\omega} \partial_{\hat{\omega}} \hat{f}_\kappa(\hat{\omega}, \hat{p}) = 0 \quad (52)$$

whose general solution has the form

$$\hat{f}_\kappa(\hat{\omega}, \hat{p}) = \frac{1}{\hat{p}^{1/2}} \hat{\zeta} \left( \frac{\hat{\omega}}{\hat{p}^{3/2}} \right) \quad (53)$$

where the function  $\hat{\zeta}$  cannot be determined from the homogeneous equation but can be extracted from the numerical solution of the full equation (by tabulating the values  $\hat{p}^{1/2} \hat{f}_\kappa(\hat{\omega}, \hat{p})$  against the ratios  $\hat{\omega}/\hat{p}^{3/2}$ ). We observe that the fixed point function  $\hat{f}_\kappa(\hat{\omega}, \hat{p})$  is regular for all  $\hat{\omega}$  and  $\hat{p}$  (see Fig. 2), which allows us to deduce the limits of  $\hat{\zeta}$ . First  $\hat{\zeta}(0)$  has to be finite for the limit  $\hat{\omega} \rightarrow 0$  to exist and followingly  $\hat{f}_\kappa \sim \hat{\zeta}(0) \hat{p}^{-1/2}$  for  $\hat{p} \gg 1$  at fixed  $\hat{\omega}$ . Second,  $\hat{\zeta}$  must behave as  $\hat{\zeta}(x) \sim \hat{\zeta}_\infty x^{-1/3}$  as  $x \rightarrow \infty$  for the limit  $\hat{p} \rightarrow 0$  to exist and followingly  $\hat{f}_\kappa \sim \hat{\zeta}_\infty \hat{\omega}^{-1/3}$  for  $\hat{\omega} \gg 1$  at fixed  $\hat{p}$ . We show below that the form of the solution (53) entails scaling for the (dimensionful) correlation function  $C(\varpi, p)$ .

We now consider the dimensionful function

$$f(\varpi, p) = D_\kappa \hat{f}(\hat{\omega}, \hat{p}) = D_\kappa \hat{f} \left( \frac{\varpi}{D_\kappa \kappa^2}, \frac{p}{\kappa} \right). \quad (54)$$

The physical limit is obtained when the running scale  $\kappa$  tends to zero at fixed values of  $\varpi$  and  $p$ . This limit is precisely equivalent to  $\hat{\omega} \gg 1$  or/and  $\hat{p} \gg 1$ , which corresponds to the scaling regime described above where  $\hat{f}$  takes the form (53). Moreover, when  $\kappa \rightarrow 0$ ,  $D_\kappa$  behaves as a power law  $D_\kappa = D_0 \kappa^{-1/2}$  where  $D_0$  is a non-universal constant. Hence, the physical dimensionful function  $f$  is expressed in terms of the scaling function  $\hat{\zeta}$  as

$$f(\varpi, p) = \frac{D_0}{p^{1/2}} \hat{\zeta} \left( \frac{1}{D_0} \frac{\varpi}{p^{3/2}} \right). \quad (55)$$

The correlation function is defined, upon inverting the matrix of the 2-point vertex functions  $\Gamma^{(2)}$ , by

$$C(\varpi, p) = - \frac{\Gamma^{(0,2)}(\varpi, p)}{[\Gamma^{(1,1)}(\varpi, p)]^2} = \frac{2f(\varpi, p)}{\varpi^2 + p^4 f(\varpi, p)^2} \quad (56)$$

where the *Ansatz* (44), with  $f_\kappa^D = f_\kappa^\nu \equiv f_\kappa$  and  $f_\kappa^\lambda \equiv 1$ , has been used in the second equality, together with  $\nu = D = 1$ . Note that the definition (56) of the correlation function corresponds in real space to the connected mean value  $\langle h(t, x) h(0, 0) \rangle_c$  which differs by a factor  $-2$  from the definition (2) in the co-moving frame. The correlation function defined by (56) with the choice  $\nu = D = 1$  finally relates to the Fourier transform of the correlation function defined by (2) with a multiplicative factor

$$C_0 = - \frac{1}{2} \frac{\nu^2}{D}. \quad (57)$$

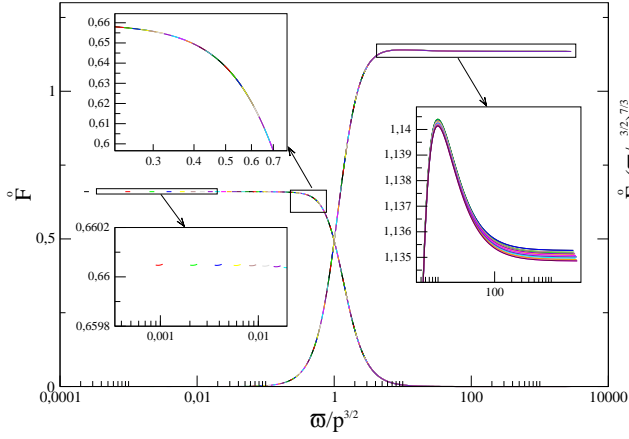


FIG. 3. (Color online) Leftmost curve: Scaling function  $\hat{F}\left(\frac{\varpi}{p^{3/2}}\right)$  corresponding to the data collapse (60), with the two insets zooming different parts to show the very high quality of the collapse (note the vertical scales); the various colors differentiate the contributions of distinct values of  $\hat{\varpi}$ . Rightmost curve: Scaling function  $\hat{F}\left(\tau = \frac{\varpi}{p^{3/2}}\right)$  multiplied by  $\tau^{7/3}$  to illustrate the power-law behavior of the tail  $\hat{F} \sim \tau^{-7/3}$  (see text). Note that the small dispersion visible in the inset zooming the tail for  $\tau \gtrsim 100$  is hence magnified by a factor of order  $100^{7/3}$ .

Replacing in (56)  $f$  by its expression (55) yields

$$C(\varpi, p) = \frac{2}{p^{7/2}} \frac{D_0 \hat{\zeta} \left( \frac{1}{D_0} \frac{\varpi}{p^{3/2}} \right)}{\varpi^2/p^3 + D_0^2 \hat{\zeta}^2 \left( \frac{1}{D_0} \frac{\varpi}{p^{3/2}} \right)} \quad (58)$$

$$= \frac{2}{p^{7/2}} \frac{1}{D_0} \frac{\hat{\zeta} \left( \frac{\hat{\varpi}}{p^{3/2}} \right)}{\hat{\varpi}^2/\hat{p}^3 + \hat{\zeta}^2 \left( \frac{\hat{\varpi}}{p^{3/2}} \right)} \quad (59)$$

$$\equiv \frac{2}{p^{7/2}} \frac{1}{D_0} \hat{F} \left( \frac{1}{D_0} \frac{\varpi}{p^{3/2}} \right). \quad (60)$$

Eq. (58) shows that the correlation function takes a scaling form at large distance and long time. Let us emphasize once more that we did not *assume* scaling, the latter emerges from the fixed-point solution of the flow equation starting from any reasonable microscopic initial condition. The scaling function  $\hat{F}$  is hence universal, up to an absolute normalisation and a rescaling of its argument by a multiplicative constant.

Eq. (59) defines how this function  $\hat{F}$  can be extracted numerically from the data for the dimensionless fixed function. We proceeded for various initial conditions and for different values of the parameter  $\alpha$ . In all cases, we observed for each value of  $\alpha$  the expected data collapse – generating the scaling function  $\hat{F}$  – with a very high precision, as illustrated in Fig. 3.

## 2. Normalisations

Our aim is now to confront our scaling function  $\hat{F}$  with the exact result obtained in Ref. [1]. The first step consists in fixing the normalisations. The universal scaling function  $g(y)$  defined below Eq. (2) is normalised in [1] in the following way:

$$g(y) = \lim_{t \rightarrow \infty} \frac{C \left( (2\lambda A t^2)^{1/3} y, t \right)}{(\frac{1}{2} \lambda A^2 t)^{2/3}} \quad (61)$$

with  $A \equiv D/\nu$ . Then three functions  $f$ ,  $\tilde{f}$  and  $\hat{f}$  are introduced in [1], through the definitions

$$\begin{aligned} f(y) &= \frac{1}{4} g''(y) \\ \tilde{f}(k) &= 2 \int_0^\infty dy \cos(ky) f(y) \\ \hat{f}(\tau) &= 2 \int_0^\infty dk \cos(k\tau) \tilde{f}(k^{2/3}) \end{aligned} \quad (62)$$

and imposing the additional normalisation condition

$$\tilde{f}(0) = 1. \quad (63)$$

The last function  $\hat{f}$  is proportional to  $C(\omega, p)/p^{7/2}$  (see [1]), that is it corresponds to our function  $\hat{F}$  reconstructed using (60) up to normalisation factors. (The analogue of the functions  $\tilde{f}$  and  $f$  are also denoted with capital letters  $\tilde{F}$  and  $F$  respectively.) The precise proportionality constant between  $\hat{F}$  and  $\hat{f}$  can be deduced from (61) and (62):

$$\hat{f}(\tau) = -\frac{p^{7/2}}{2^{5/3} \lambda^{4/3} A^{5/3} t^{7/3}} C \left( \frac{p}{(2\lambda A t^2)^{1/3}}, \tau \frac{p^{3/2}}{t} \right). \quad (64)$$

Comparing this expression with our definition (60) and taking into account the multiplicative factor (57), we obtain the relation

$$\hat{f}(\tau) = 2\sqrt{2g^*} \sqrt{\frac{D}{\nu A}} \hat{F} \left( \sqrt{2g^*} \sqrt{\frac{\nu A}{D}} \tau \right) \quad (65)$$

where we used that the bare value  $\lambda$  is related to the fixed point coupling  $g^*$  through  $g^* = g_b/D_0^2 = \lambda^2 D/(D_0^2 \nu^3)$ . Relating the Fourier transforms is then straightforward:

$$\tilde{f}(k) = 2 \frac{D}{\nu A} \tilde{F} \left( \frac{k}{(2g^* \frac{\nu A}{D})^{1/3}} \right) \equiv \frac{1}{\tilde{F}_n} \tilde{F} \left( \frac{k}{k_n} \right). \quad (66)$$

Finally, using the same normalisation criterion (63) as in [1] gives the absolute vertical normalisation  $\tilde{F}_n = \frac{\nu A}{2D} = \tilde{F}(0)$  and the absolute horizontal normalisation  $k_n = (4\tilde{F}_n g^*)^{1/3}$ .

### 3. Properties of the scaling function $\tilde{f}$

Let us first compare the scaling functions  $\tilde{f}$  and  $\tilde{F}$ . The function  $\tilde{f}$  is studied in details in [1] and also in [17, 44], where interesting features are highlighted. According to Ref. [1], the function  $\tilde{f}$  first decreases to vanish at  $k_0 \simeq 4.36236\dots$  and then exhibits a negative dip of coordinates ( $k_d \simeq 4.79079\dots$ ,  $\tilde{f}_d \simeq -0.0012023\dots$ ). After this dip, the function decays to zero with a stretched exponential tail, over which are superimposed tiny oscillations around zero, only apparent on a logarithmic scale. A heuristic fit of this behavior for  $k \gtrsim 15$  is given in [1]

$$\tilde{f}(k) \sim 10.9k^{-9/4} \sin\left(\frac{k^{3/2}}{2} - 1.937\right) e^{-\frac{1}{2}k^{3/2}}. \quad (67)$$

We show below that we here recover qualitatively all these features, with reasonable estimates for the different parameters that characterize them. Our function  $\tilde{F}$  is defined from  $\tilde{F}$  by the integral

$$\tilde{F}(k) = \int_0^\infty \frac{d\tau}{\pi} \cos(\tau k^{3/2}) \tilde{F}(\tau) \quad (68)$$

which has to be computed numerically. The function  $\tilde{F}$  stems from the superposition of the numerous curves involved in the data collapse of Eq. (60). Although the data collapse is excellent, there subsists a high frequency and small amplitude noise due to the re-ordering of the points (apparent upon a large zoom as presented in the insets of Fig. 3). As we are willing to investigate the properties of the tail of  $\tilde{F}$  with high precision, we first need to eliminate this noise. For that, we device an appropriate family of analytical fitting functions to smooth our data for  $\tilde{F}(\tau)$ . The choice of the family of fitting functions is determined as follows.

First, they have to reproduce the large  $\tau$  behavior of  $\tilde{F}$ . The latter can be inferred from the limits of the function  $\hat{\zeta}(x)$  established after Eq. (53), one obtains  $\tilde{F}(\tau) \rightarrow \tilde{F}_\infty \tau^{-7/3}$ . For each value of the parameter  $\alpha$ , the proportionality constant  $\tilde{F}_\infty$  can be estimated graphically (up to 4-5 digits) from the curve  $\tau^{7/3} \tilde{F}(\tau)$ . Moreover, the fitting functions have to be even, and finite at the origin. To satisfy these constraints, we build a family of fitting functions as an expansion in elementary rational polynomials of  $\tau^2$  raised to the adequate power to reproduce the large  $\tau$  behavior:

$$\tilde{F}_{\text{fit}}(\tau) = \left( \frac{a_{00} + a_{02}\tau^2}{1 + a_{01}\tau^2 + a_{03}\tau^4} + \frac{a_{10}}{1 + a_{11}\tau^2} + \frac{a_{20}}{1 + a_{21}\tau^2} + \dots \right)^{7/6} \quad (69)$$

with the additional constraint  $(a_{02}/a_{03} + a_{10}/a_{11} + a_{20}/a_{21} + \dots)^{6/7} = \tilde{F}_\infty$  [45]. The first fit is achieved using the three independent coefficients  $a_{0i}$ . The corresponding denominator introduces four non-analyticities

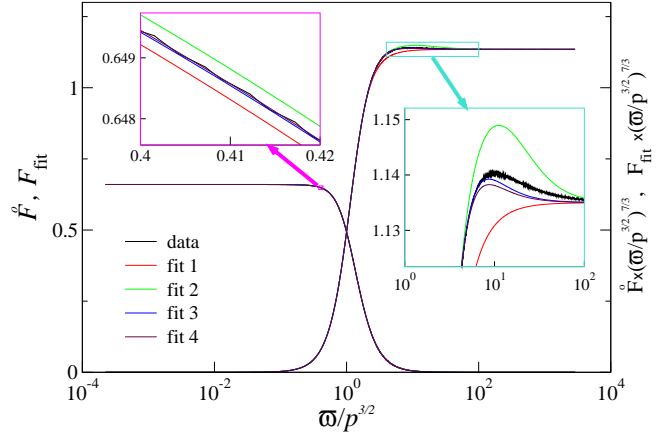


FIG. 4. (Color online) Illustration of the fitting procedure described in the text, using the same data for  $\tilde{F}$  as in Fig. 3 but with unified colors (black curves: on the left  $\tilde{F}(\tau)$ ; on the right  $\tilde{F}(\tau)\tau^{7/3}$ ). The four successive orders of the fit appear superimposed in the main graph; the two insets present large zooms (note the vertical scales) to separate them and evidence the convergence: the higher the order, the closer to the data the fit lies. Note that for the right curve  $\tilde{F}(\tau)\tau^{7/3}$  the differences are again magnified by a factor  $\tau^{7/3}$ .

in the points of the complex plane  $\pm z_0^\pm$  with

$$z_0^\pm = \sqrt{\frac{1}{2a_{03}} \left( -a_{01} \pm i\sqrt{-a_{01}^2 + 4a_{03}} \right)} \quad (70)$$

whose coordinates were found to be very robust against the choice and the order of the fit as evidenced below. Note that these four points appeared never to lie on the imaginary axis, nor on the real axis ( $-a_{01}^2 + 4a_{03} > 0$ ). We then add in turn simple monomials corresponding to purely imaginary poles up to nine independent coefficients (we observed that additional complex poles were systematically decomposed into two purely imaginary poles). This procedure turned out to converge rapidly for all  $\alpha$  values, as illustrated in Fig. 4. In particular, the existence and the coordinates of the complex singularities  $\pm z_0^\pm$  appeared to be a robust feature of the data. Moreover, they are always found to lie the closest to the real axis [46]. For the remaining calculations we work with the analytical expression  $\tilde{F}_{\text{fit}}$  which reproduces faithfully our data, and hence drop in the following the index  $\text{fit}$ .

We computed numerically the function  $\tilde{F}$  from  $\tilde{F}_{\text{fit}}$  according to (68) and normalized it using (66), which yielded the following results. We find that  $\tilde{F}$  exhibits all the qualitative features of the exact function  $\tilde{f}$ , in particular the existence of the negative dip and the subsequent stretched exponential decay with the presence of oscillations in the tail, as displayed in Fig. 5. Moreover, it compares quite accurately with the exact function. Indeed, we find for the position of the first zero  $k_0 \simeq 4.28(2)$  and for the coordinates of the dip ( $k_d \simeq 5.15(3)$ ,  $\tilde{f}_d \simeq -0.013(1)$ ), which are reasonably

close to the exact results, see Table II. As for the behavior of the tail of  $\tilde{F}$ , it can be inferred analytically from the pole structure of  $\hat{F}$ . Let us define  $\bar{F}(k) = \tilde{F}(k^{2/3})$ , which is hence the standard Fourier transform of  $\hat{F}$

$$\bar{F}(k) = \int_0^\infty \frac{d\tau}{\pi} \cos(\tau k) \hat{F}(\tau). \quad (71)$$

As  $\hat{F}(\tau)$  is  $C^\infty$ , the tail of  $\bar{F}$  is dominated by the singularities of  $\hat{F}(\tau)$  in the upper complex half plane lying the closest to the real axis, which are  $z_0^+$  and  $-z_0^-$ . Denoting  $z_0^+ = a_0 + ib_0$  with  $b_0 > 0$ , we obtain  $\bar{F}(k) \sim e^{-ikz_0^+} + e^{ikz_0^-} \propto e^{-b_0 k} \cos(a_0 k)$  as  $k \rightarrow \infty$  and followingly

$$\tilde{F}(k) \sim \bar{F}(k^{3/2}) \sim e^{-b_0 k^{3/2}} \cos(a_0 k^{3/2}) \quad \text{as } k \rightarrow \infty. \quad (72)$$

$\tilde{F}$  hence decays following a stretched exponential with superimposed oscillations on the scale  $k^{3/2}$  exactly as observed in the exact solution (see (67)). Regarding the tiny magnitude over which develop these features, this agreement is remarkable. Let us emphasize that within the MC approximation, the stretched exponential behavior and the oscillations were evidenced, but not on the correct scale [1, 17]. The NPRG method hence provides more accurate results than the MC approach, and with much less inputs (no assumed scaling nor a precise scaling form).

A consequence is that, conversely to the MC approach, the coefficient of the exponential and the period of the oscillations can here be estimated – extracted analytically from the values of  $z_0$ . We find  $b_0 \simeq 0.33(1)$  for the coefficient of the exponential, and  $a_0 \simeq 0.17(1)$  for the pulsation of the oscillations (checking that these values coincide with the same quantities estimated graphically from the tail of  $\tilde{F}$  computed numerically – the latter being determined with much less accuracy). These coefficients can be compared with the coefficients of the fit (67) of the tail of the exact function which gives  $b_0 = a_0 = \frac{1}{2}$ . They are of the same order, which is already highly non-trivial. The discrepancy is visible on a logarithmic scale, as illustrated in the inset of Fig. 5.

#### 4. Scaling function in real space and universal amplitude ratio

We finally come to the real space scaling function  $f$  defined in (62). We computed it numerically by Fourier transforming  $\tilde{F}$

$$F(y) = \int_0^\infty \frac{dk}{\pi} \cos(ky) \tilde{F}(k). \quad (73)$$

It is compared in Fig. 6 with the exact result. Again, our function reproduces quite accurately the exact one, though it is the less accurate of our three scaling functions since it follows from two successive numerical (oscillating)

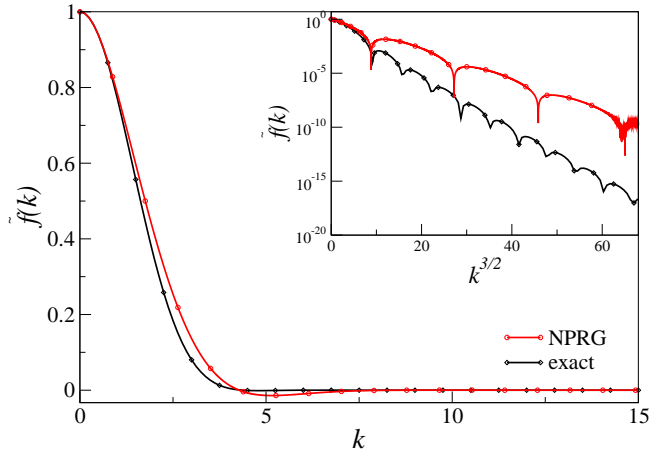


FIG. 5. (Color online) Comparison of the scaling function  $\tilde{F}(k)$  (red curve) obtained in this work with the exact result  $\tilde{f}(k)$  (black curve) from [1]. The inset shows the stretched exponential behavior of the tail with the superimposed oscillations. Note the vertical scale: this behavior develops with amplitudes below typically  $10^{-6}$  (see text for a detailed comment of the figure).

integrations of our raw data. The tail is particularly sensitive to this loss of precision. The exact function  $f(y)$  is found to decrease as  $\exp(-cy^3)$  when  $y \rightarrow \infty$  in [1], whereas the decay of our function  $F(y)$ , though it starts with the correct behavior, rapidly crosses over to a simple exponential decay  $\exp(-c'y)$ .

From this function can be computed the universal amplitude ratio  $g_0$  with the definition given in [1]

$$g_0 \equiv 4 \int_0^\infty dy y f(y). \quad (74)$$

The exact result is  $g_0 = 1.1503944783\dots$  (more digits can be found in [1]). Here, the universal constant  $g_0$  can be estimated by performing the numerical integration corresponding to (74) using  $F$ . However, this amounts to achieve three successive numerical integrations from our raw function  $\tilde{F}$  and the resulting precision is low. Instead, one can compute part of the involved integrals analytically, using the definition given in [1]:  $g_0 \equiv g(0)$  where  $g(y)$  is the original scaling function proportional to the second derivative of  $f(y)$  (see (62)). Indeed,  $g(y)$  can be expressed in term of the Fourier transform  $\tilde{f}$  of  $f$  and one gets

$$g(0) = \lim_{y \rightarrow \infty} -\frac{4}{\pi} \int_0^\infty dk (1 - \cos(ky)) \left( \frac{\tilde{f}(k) - 1}{k^2} \right). \quad (75)$$

Since the function  $(\tilde{f}(k) - 1)/k^2$  is infinitely derivable, its Fourier transform vanishes in the limit  $y \rightarrow \infty$  and one



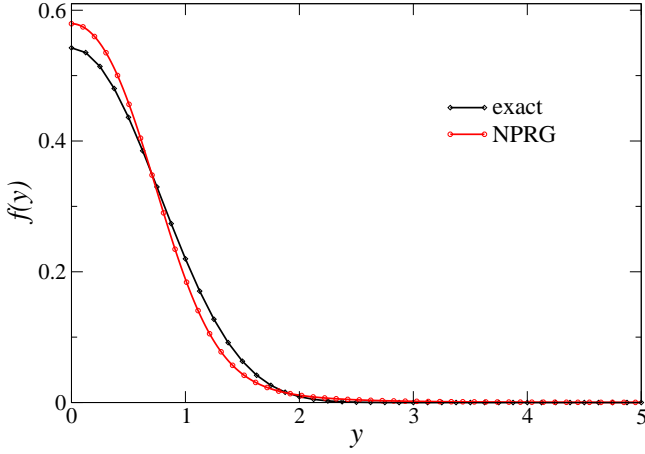


FIG. 6. (Color online) Comparison of the scaling function  $F(y)$  (red curve) obtained in this work with the exact result  $f(y)$  (black curve) from [1].

quantity	exact	NPRG
$g_0$	1.15039	1.13(2)
$k_0$	4.36236	4.28(2)
$k_d$	4.79079	5.15(3)
$\tilde{f}_d$	-0.00120	-0.013(1)
$a_0$	$\frac{1}{2}$	0.17(1)
$b_0$	$\frac{1}{2}$	0.33(1)
$\omega$	—	0.82(4)

TABLE II. Characteristic parameters of the different scaling functions, from the exact result [1] and from this work: i) relative to  $f$ , universal amplitude ratio  $g_0$ ; ii) relative to  $\tilde{f}$ : position of the first zero  $k_0$ , coordinates of the negative dip ( $k_d, \tilde{f}_d$ ), coefficient of the stretched exponential  $b_0$ , pulsation of the oscillations  $a_0$ ; iii) correction to scaling exponent  $\omega$ .

is left with

$$g(0) = -\frac{4}{\pi} \int_0^\infty dk \left( \frac{\tilde{f}(k) - 1}{k^2} \right) \quad (76)$$

$$= \frac{6}{\pi^2} \int_0^\infty \frac{dk}{\sqrt{k}} \int_0^\infty d\tau \sin(\tau k^{3/2}) \tau \tilde{f}(\tau) \quad (77)$$

$$= \frac{2}{\pi^2} \Gamma\left(\frac{1}{3}\right) \int_0^\infty d\tau \tau^{2/3} \tilde{f}(\tau). \quad (78)$$

This universal quantity can thus be alternatively determined numerically with much higher precision by performing a unique, non-oscillating integral. We find  $g_0 \simeq 1.13(2)$  which is in close agreement with the exact value, slightly superior to the MC estimate  $g_0 \simeq 1.1137$  [17] (though the latter does not provide any estimate of the error). All our estimates for the characteristic parameters of the different scaling functions obtained in this section are summarized in Table II.

## VII. CONCLUSION

In this work, we have presented the general framework to investigate the KPZ equation using the NPRG method. We have proposed a detailed analysis of the symmetries of the KPZ equation, both the standard symmetries – Galilean and shift – and their versions gauged in time, and the one-dimensional time-reversal symmetry. We have derived general Ward identities associated with these symmetries and proposed a convenient geometric interpretation of the Galilean symmetry in terms of covariant time derivatives. We have then devised an approximation scheme based on an *Ansatz* for  $\Gamma_\kappa$  which, conversely to the standard derivative expansion often used, preserves the momentum structure of the vertex functions. This *Ansatz*, which is strongly constrained by the symmetries, has allowed us to compute correlation functions in a non-perturbative, yet systematically improvable, way.

We implemented the minimal order in the response field of this approximation scheme. We found that, without any input other than the bare action and its symmetries (in particular without assuming scaling), the renormalization group flow is generically attracted towards a strong-coupling fixed point – which roots the existence of generic scaling – or to the EW fixed point for  $d > 2$  and  $\lambda < \lambda_c$ , yielding for the first time the full correct phase diagram of the KPZ equation within a RG approach.

We specifically developed two applications: the determination of critical exponents in physical dimensions with a simplified *Ansatz* and the computation of universal scaling functions in one-dimension. The estimates of the critical exponents obtained in dimensions two and three compare reasonably with results from simulations, though the accuracy decreases with the dimension so that we are unable, at this order, to settle on the existence of an upper critical dimension. The scaling functions  $\tilde{F}$ ,  $\tilde{F}$  and  $F$  obtained in one-dimension compare very accurately with the exact results. In particular, we are able to recover the stretched exponential with tiny superimposed oscillations of the tail of  $\tilde{f}(k)$  on the correct scale  $k^{3/2}$ . We also obtained an accurate estimate of the universal amplitude ratio  $g_0$ . Quantities beyond the scaling regime can also be computed, which we illustrated here with the correction to scaling exponent  $\omega$ .

A further step will consist in refining the computation of critical exponents in all dimensions by improving the approximation, which is in progress. One could also compute the probability distributions, which are again known exactly in one dimension but not in any others, and investigate the influence of initial conditions. This requires a further theoretical development to take into account the initial conditions. We believe that we have provided a solid theoretical framework to study the strong-coupling phase of the KPZ equation, as well as other non-perturbative and out-of-equilibrium problems.

## ACKNOWLEDGMENTS

L. Canet wishes to thank the Universidad de la República for fundings and hospitality during important stages of this work. The authors also wish to thank R. Blanch for his help to optimize the numerical codes and paralelize them, M. Prähofer and H. Spohn for providing

us with their data for the scaling function  $f$  and its fourier transform  $\tilde{f}$ , and M. Moore for discussions concerning the MC results. N. Wschebor acknowledges the support of PEDECIBA and ANII-FCE. The numerical parallel codes were run on the clusters FING and PEDECIBA (Montevideo) and on the cluster Healthphy (CIMENT, Grenoble).

## APPENDIX A: TIME-REVERSAL WARD IDENTITIES FOR THE 3- AND 4-POINT FUNCTIONS

All the Ward identities for the 3- and 4-point vertex functions are derived by taking functional derivatives of the identity (37) and evaluating the result at uniform and static fields. For the remaining 3-point function, one obtains in Fourier space:

$$2\Gamma_{\kappa}^{(3,0)}(\omega_1, \vec{p}_1; \omega_2, \vec{p}_2) = -\frac{\nu}{D} p_1^2 \text{Re}\Gamma_{\kappa}^{(2,1)}(\omega_2, \vec{p}_2; -\omega_1 - \omega_2, -\vec{p}_1 - \vec{p}_2) - \frac{\nu}{D} p_2^2 \text{Re}\Gamma_{\kappa}^{(2,1)}(\omega_1, \vec{p}_1; -\omega_1 - \omega_2, -\vec{p}_1 - \vec{p}_2) \\ - \frac{\nu}{D} p_3^2 \text{Re}\Gamma_{\kappa}^{(2,1)}(\omega_1, \vec{p}_1; \omega_2, \vec{p}_2) + \frac{1}{2} \left( \frac{\nu}{D} \right)^3 p_1^2 p_2^2 p_3^2 \Gamma_{\kappa}^{(0,3)}(\omega_1, \vec{p}_1; \omega_2, \vec{p}_2). \quad (79)$$

For the 4-point functions, we report the four additional independent identities obtained for uniform and static fields:

$$2\text{Re}\Gamma_{\kappa}^{(1,3)}(\omega_1, \omega_2, \omega_3) = -\frac{\nu}{D} p_1^2 \Gamma_{\kappa}^{(0,4)}(\omega_1, \omega_2, \omega_3) \\ 2\text{Im}\Gamma_{\kappa}^{(2,2)}(\omega_1, \omega_2, \omega_3) = -\frac{\nu}{D} p_2^2 \text{Im}\Gamma_{\kappa}^{(1,3)}(\omega_1, \omega_2, \omega_3) - \frac{\nu}{D} p_1^2 \text{Im}\Gamma_{\kappa}^{(1,3)}(\omega_2, \omega_1, \omega_3) \\ 2\text{Re}\Gamma_{\kappa}^{(3,1)}(\omega_4, \omega_3, \omega_2) = \frac{1}{2} \left( \frac{\nu}{D} \right)^3 p_2^2 p_3^2 p_4^2 \Gamma_{\kappa}^{(0,4)}(\omega_4, \omega_3, \omega_2) - \frac{\nu}{D} p_4^2 \text{Re}\Gamma_{\kappa}^{(2,2)}(\omega_3, \omega_2, \omega_4) - \frac{\nu}{D} p_3^2 \text{Re}\Gamma_{\kappa}^{(2,2)}(\omega_2, \omega_4, \omega_3) \\ - \frac{\nu}{D} p_2^2 \text{Re}\Gamma_{\kappa}^{(2,2)}(\omega_3, \omega_4, \omega_2) \quad (80)$$

and finally

$$p_1^2 \text{Im}\Gamma_{\kappa}^{(3,1)}(\omega_2, \omega_3, -\omega_1 - \omega_2 - \omega_3) + 3 \text{ perm.} = -\frac{1}{2} \left( \frac{\nu}{D} \right)^2 p_1^2 p_2^2 p_3^2 \text{Im}\Gamma_{\kappa}^{(1,3)}(-\omega_1 - \omega_2 - \omega_3, \omega_1, \omega_2) + 3 \text{ perm.} \quad (81)$$

## APPENDIX B: $n$ -POINT FUNCTIONS AT THE MINIMAL ORDER OF THE APPROXIMATION SCHEME

To compute 3- and 4- point functions at vanishing field, one needs to take functional derivatives of the functions  $f_{\kappa}^X(-\tilde{D}_t^2, -\nabla^2)$  ( $X = D, \nu, \lambda$ ) with respect to the field  $\varphi$  and then evaluate the result at  $\varphi = 0$ . This can be done using the expression of the series expansion (43):

$$\frac{\delta f_{\kappa}^X(-\tilde{D}_t^2, -\nabla^2)}{\delta \varphi(t_1, \vec{x}_1)} = \sum_{m=1, n=0}^{\infty} a_{mn} \sum_{k=0}^{m-1} (-\tilde{D}_t^2)^k \frac{\delta(-\tilde{D}_t^2)}{\delta \varphi(t_1, \vec{x}_1)} (-\tilde{D}_t^2)^{m-k-1} (-\nabla_x^2)^n \quad (82)$$

with

$$\frac{\delta(-\tilde{D}_t^2)}{\delta \varphi(t_1, \vec{x}_1)} = \lambda \left( \nabla_x (\delta(t - t_1) \delta^{(d)}(\vec{x} - \vec{x}_1)) \cdot \nabla_x (\partial_t - \lambda \nabla_x \varphi(\mathbf{x}) \cdot \nabla_x) \right. \\ \left. + (\partial_t - \lambda \nabla_x \varphi(\mathbf{x}) \cdot \nabla_x) (\nabla_x (\delta(t - t_1) \delta^{(d)}(\vec{x} - \vec{x}_1)) \cdot \nabla_x) \right). \quad (83)$$

When Fourier transforming,

$$\frac{\delta(-\tilde{D}_t^2)}{\delta \varphi(t_1, \vec{x}_1)} \rightarrow i \lambda \vec{p}_1 \cdot (\vec{p}_1 + \vec{p}) (\omega_1 + 2\omega) \quad (84)$$

One obtains for instance

$$\Gamma_{\kappa}^{(1,2)}(\omega_1, \vec{p}_1, \omega_2, \vec{p}_2) = -i\lambda \sum_{m=1, n=0}^{\infty} a_{mn} \times \sum_{k=0}^{m-1} \omega_2^{2k} [\vec{p}_1 \cdot (\vec{p}_1 + \vec{p}_2)(\omega_1 + 2\omega_2)] (\omega_1 + \omega_2)^{2(m-k-1)} ((\vec{p}_1 + \vec{p}_2)^2)^n + (2 \leftrightarrow 3). \quad (85)$$

and thus:

$$\begin{aligned} \Gamma_{\kappa}^{(1,2)}(\omega_1, \vec{p}_1, \omega_2, \vec{p}_2) = & -\frac{i\lambda}{\omega_1} [\vec{p}_1 \cdot (\vec{p}_1 + \vec{p}_2) (f_{\kappa}^D((\omega_1 + \omega_2)^2, (\vec{p}_1 + \vec{p}_2)^2) - f_{\kappa}^D(\omega_2^2, (\vec{p}_1 + \vec{p}_2)^2)) \\ & - \vec{p}_1 \cdot \vec{p}_2 (f_{\kappa}^D(\omega_2^2, \vec{p}_2^2) - f_{\kappa}^D((\omega_1 + \omega_2)^2, \vec{p}_2^2))] . \end{aligned} \quad (86)$$

All the other functions can be computed the same way. The 3-point functions write

$$\Gamma_{\kappa}^{(3,0)}(\omega_1, \omega_2; \vec{p}_1, \vec{p}_2) = 0 \quad (87)$$

$$\Gamma_{\kappa}^{(0,3)}(\omega_1, \omega_2; \vec{p}_1, \vec{p}_2) = 0 \quad (88)$$

$$\begin{aligned} \Gamma_{\kappa}^{(2,1)}(\omega_1, \omega_2; \vec{p}_1, \vec{p}_2) = & \lambda \vec{p}_1 \cdot \vec{p}_2 f_{\kappa}^{\lambda}((\omega_1 + \omega_2)^2, (\vec{p}_1 + \vec{p}_2)^2) + \lambda \vec{p}_1 \cdot \vec{p}_2 \frac{\omega_1}{\omega_2} [f_{\kappa}^{\lambda}((\omega_1 + \omega_2)^2, \vec{p}_1^2) - f_{\kappa}^{\lambda}(\omega_1^2, \vec{p}_1^2)] \\ & + \lambda \vec{p}_1 \cdot \vec{p}_2 \frac{\omega_2}{\omega_1} [f_{\kappa}^{\lambda}((\omega_1 + \omega_2)^2, \vec{p}_2^2) - f_{\kappa}^{\lambda}(\omega_2^2, \vec{p}_2^2)] \\ & + i\lambda \frac{\nu}{2D} \left\{ \vec{p}_1^2 \frac{\vec{p}_2}{\omega_2} \cdot (\vec{p}_1 + \vec{p}_2) \left[ f_{\kappa}^{\nu}((\omega_1 + \omega_2)^2, (\vec{p}_1 + \vec{p}_2)^2) - f_{\kappa}^{\nu}(\omega_1^2, (\vec{p}_1 + \vec{p}_2)^2) \right] \right. \\ & + \vec{p}_1^2 \frac{\vec{p}_2}{\omega_2} \cdot \vec{p}_1 \left[ f_{\kappa}^{\nu}((\omega_1 + \omega_2)^2, \vec{p}_1^2) - f_{\kappa}^{\nu}(\omega_1^2, \vec{p}_1^2) \right] + \vec{p}_2^2 \frac{\vec{p}_1}{\omega_1} \cdot \vec{p}_2 \left[ f_{\kappa}^{\nu}((\omega_1 + \omega_2)^2, \vec{p}_2^2) - f_{\kappa}^{\nu}(\omega_2^2, \vec{p}_2^2) \right] \\ & \left. + \vec{p}_2^2 \frac{\vec{p}_1}{\omega_1} \cdot (\vec{p}_1 + \vec{p}_2) \left[ f_{\kappa}^{\nu}((\omega_1 + \omega_2)^2, (\vec{p}_1 + \vec{p}_2)^2) - f_{\kappa}^{\nu}(\omega_2^2, (\vec{p}_1 + \vec{p}_2)^2) \right] \right\}. \end{aligned} \quad (89)$$

Note that the combinations appearing in  $\Gamma_{\kappa}^{(2,1)}$  and  $\Gamma_{\kappa}^{(1,2)}$  are related. If one denotes  $\Gamma_{\kappa, D}^{(1,2)}$  where the  $D$  index labels the function ( $f_{\kappa}^D$ ) appearing in the expression, one has

$$i\text{Im}\Gamma_{\kappa}^{(2,1)}(\omega_1, \omega_2; \vec{p}_1, \vec{p}_2) = -\frac{\nu}{2D} \left\{ \vec{p}_1^2 \Gamma_{\kappa, \nu}^{(1,2)}(\omega_2, \omega_1; \vec{p}_2, \vec{p}_1) + \vec{p}_2^2 \Gamma_{\kappa, \nu}^{(1,2)}(\omega_1, \omega_2; \vec{p}_1, \vec{p}_2) \right\}. \quad (90)$$

where the  $\nu$  index in  $\Gamma_{\kappa, \nu}^{(1,2)}$  indicates that  $f_{\kappa}^D$  is replaced by  $f_{\kappa}^{\nu}$  in expression (86). This type of relation is used in the following to shorten the expression of  $\Gamma_{\kappa}^{(3,1)}$ . The 4-point functions are

$$\begin{aligned} \Gamma_{\kappa}^{(4,0)}(\omega_1, \omega_2, \omega_3; \vec{p}_1, \vec{p}_2, \vec{p}_3) &= 0 \\ \Gamma_{\kappa}^{(1,3)}(\omega_1, \omega_2, \omega_3; \vec{p}_1, \vec{p}_2, \vec{p}_3) &= 0 \\ \Gamma_{\kappa}^{(0,4)}(\omega_1, \omega_2, \omega_3; \vec{p}_1, \vec{p}_2, \vec{p}_3) &= 0 \\ \Gamma_{\kappa}^{(2,2)}(\omega_1, \omega_2, \omega_3; \vec{p}_1, \vec{p}_2, \vec{p}_3) &= -\lambda^2 \vec{p}_1 \cdot (\vec{p}_1 + \vec{p}_3) \vec{p}_2 \cdot \vec{p}_4 \left[ \frac{f_{\kappa}^D((\omega_4^2, \vec{p}_4^2)}{(\omega_1 + \omega_2)\omega_2} + \frac{f_{\kappa}^D(\omega_3^2, \vec{p}_4^2)}{(\omega_1 + \omega_2)\omega_1} - \frac{f_{\kappa}^D((\omega_1 + \omega_3)^2, \vec{p}_4^2)}{\omega_1\omega_2} \right] \\ &\quad - \lambda^2 \vec{p}_2 \cdot (\vec{p}_2 + \vec{p}_3) \vec{p}_1 \cdot \vec{p}_4 \left[ \frac{f_{\kappa}^D((\omega_4^2, \vec{p}_4^2)}{(\omega_1 + \omega_2)\omega_1} + \frac{f_{\kappa}^D(\omega_3^2, \vec{p}_4^2)}{(\omega_1 + \omega_2)\omega_2} - \frac{f_{\kappa}^D((\omega_2 + \omega_3)^2, \vec{p}_4^2)}{\omega_1\omega_2} \right] \\ &\quad - \lambda^2 \vec{p}_1 \cdot (\vec{p}_1 + \vec{p}_4) \vec{p}_2 \cdot \vec{p}_3 \left[ \frac{f_{\kappa}^D((\omega_3^2, \vec{p}_3^2)}{(\omega_1 + \omega_2)\omega_2} + \frac{f_{\kappa}^D(\omega_4^2, \vec{p}_3^2)}{(\omega_1 + \omega_2)\omega_1} - \frac{f_{\kappa}^D((\omega_1 + \omega_4)^2, \vec{p}_3^2)}{\omega_1\omega_2} \right] \\ &\quad - \lambda^2 \vec{p}_2 \cdot (\vec{p}_2 + \vec{p}_4) \vec{p}_1 \cdot \vec{p}_3 \left[ \frac{f_{\kappa}^D((\omega_3^2, \vec{p}_3^2)}{(\omega_1 + \omega_2)\omega_1} + \frac{f_{\kappa}^D(\omega_4^2, \vec{p}_3^2)}{(\omega_1 + \omega_2)\omega_2} - \frac{f_{\kappa}^D((\omega_2 + \omega_4)^2, \vec{p}_3^2)}{\omega_1\omega_2} \right] \\ &\equiv \Gamma_{\kappa, D}^{(2,2)}(\omega_1, \omega_2, \omega_3; \vec{p}_1, \vec{p}_2, \vec{p}_3) \end{aligned} \quad (91)$$

where in the last line the  $D$  index refers to the involved function  $f_{\kappa}^D$ . We denote  $\bar{\Gamma}_{\kappa, D}^{(2,2)}$  the two last lines of (91) with the same convention for the meaning of the index  $D$ . Finally, one finds, omitting the dependence in  $\vec{p}_i$  (which follows



the same order as  $\omega_i$ ):

$$\begin{aligned}
\Gamma_{\kappa}^{(3,1)}(\omega_1, \omega_2, \omega_3) = & -\frac{\nu}{2D} \vec{p}_3^2 \Gamma_{\kappa, \nu}^{(2,2)}(\omega_1, \omega_2, \omega_3) - \frac{\nu}{2D} \vec{p}_2^2 \Gamma_{\kappa, \nu}^{(2,2)}(\omega_3, \omega_1, \omega_2) - \frac{\nu}{2D} \vec{p}_1^2 \Gamma_{\kappa, \nu}^{(2,2)}(\omega_2, \omega_3, \omega_1) \\
& + i\omega_3 \bar{\Gamma}_{\kappa, \lambda}^{(2,2)}(\omega_1, \omega_2, \omega_3) + i\omega_2 \bar{\Gamma}_{\kappa, \lambda}^{(2,2)}(\omega_3, \omega_1, \omega_2) + i\omega_1 \bar{\Gamma}_{\kappa, \lambda}^{(2,2)}(\omega_2, \omega_3, \omega_1) \\
& - i \frac{\lambda^2}{\omega_3} \vec{p}_3 \cdot (\vec{p}_1 + \vec{p}_2) \vec{p}_1 \cdot \vec{p}_2 \left[ f_{\kappa}^{\lambda} \left( (\omega_1 + \omega_2)^2, (\vec{p}_1 + \vec{p}_2)^2 \right) - f_{\kappa}^{\lambda} \left( \omega_4^2, (\vec{p}_1 + \vec{p}_2)^2 \right) \right] \\
& - i \frac{\lambda^2}{\omega_1} \vec{p}_1 \cdot (\vec{p}_2 + \vec{p}_3) \vec{p}_2 \cdot \vec{p}_3 \left[ f_{\kappa}^{\lambda} \left( (\omega_2 + \omega_3)^2, (\vec{p}_2 + \vec{p}_3)^2 \right) - f_{\kappa}^{\lambda} \left( \omega_4^2, (\vec{p}_2 + \vec{p}_3)^2 \right) \right] \\
& - i \frac{\lambda^2}{\omega_2} \vec{p}_2 \cdot (\vec{p}_1 + \vec{p}_3) \vec{p}_1 \cdot \vec{p}_3 \left[ f_{\kappa}^{\lambda} \left( (\omega_1 + \omega_3)^2, (\vec{p}_1 + \vec{p}_3)^2 \right) - f_{\kappa}^{\lambda} \left( \omega_4^2, (\vec{p}_1 + \vec{p}_3)^2 \right) \right]
\end{aligned} \tag{92}$$

### APPENDIX C: PROCEDURE FOR THE NUMERICAL INTEGRATION

This appendix is devoted to presenting the details of the numerical procedure implemented to achieve the integration of flow equations. We discretized the momentum and frequency on a  $\hat{p} \times \sqrt{\hat{\omega}}$  mesh of spacing  $\Delta\hat{p}$  and  $\Delta\sqrt{\hat{\omega}}$  and sizes  $\hat{p}_{\max}$  and  $\sqrt{\hat{\omega}_{\max}}$ . The integrals over the internal momentum  $\hat{q}$  and frequency  $\hat{\omega}$  are performed using Simpson's rule. The  $\sqrt{\hat{\omega}}$  mesh is chosen because the integrand can have rather long tails in  $\hat{\omega}$  as there is no cutoff term (analogous to  $r(y)$ ) suppressing the high frequencies. The values of  $\hat{f}$  at  $\hat{\omega} \pm \hat{\omega}$  which do not fall on  $\sqrt{\hat{\omega}}$  mesh points are evaluated using cubic interpolations. The function  $\hat{f}$  is extended outside the grid (for momenta  $\hat{p} + \hat{q}$  greater than  $\hat{p}_{\max}$  or/and frequencies  $\hat{\omega} + \hat{\omega}$  greater than  $\hat{\omega}_{\max}$ ) using power law extrapolations.

Regarding the integration over  $\hat{q}$ , as the integrand falls off exponentially due to the  $\partial_s S_{\kappa}$  term (derivative of the regulator), the bounds  $\pm\infty$  of the integral can be safely replaced by  $\pm\hat{p}_{\max}$ . This is not the case for the integral over the frequency  $\hat{\omega}$  as the decay of the integrand may

be slow. We first compute the integral on  $[-\hat{\omega}_{\max}, \hat{\omega}_{\max}]$  and then evaluate the contribution of the integral on the boundaries  $[-\infty, -\hat{\omega}_{\max}]$  and  $[\hat{\omega}_{\max}, \infty]$  by performing in these regions the change of variable  $x = \hat{\omega}/\hat{\omega}_{\max}$  and using the extrapolated values of  $\hat{f}$ . The precision on the momentum and frequency integral is of order  $10^{-4}$  for the typical resolutions  $\Delta\hat{p} = \Delta\sqrt{\hat{\omega}} = 1/4$  and mesh sizes  $\hat{\omega}_{\max} = 15^2$  and  $\hat{p}_{\max}$  from 20 to 40 increasing with the value of  $\alpha$  (20 for  $\alpha = 0.5$  to 40 for  $\alpha = 10$ ). The derivative terms  $\hat{p}\partial_{\hat{p}}$  and  $\hat{\omega}\partial_{\hat{\omega}}$  are computed using 5-point differences.

We use an explicit Euler time stepping with a typical time step  $\Delta s = -5.10^{-5}$  to integrate the flow equations on the renormalisation time  $s$ , which turns out to be stable. In all cases, a fixed point is reached after  $s \gtrsim -20$ . The fixed point functions are recorded at  $s = -25$ . We studied separately the influence of the resolution (values of  $\Delta\hat{p}$  and  $\Delta\sqrt{\hat{\omega}}$ ), and of the mesh sizes ( $\hat{p}_{\max}$  and  $\hat{\omega}_{\max}$ ) on the precision level, and checked the convergence. The differences (in all physical quantities) between resolutions and/or domain sizes are in all cases smaller than 1% and this numerical errors are dominated by the residual variations observed when varying the cut-off parameter  $\alpha$ , which are of order 5%.

- 
- [1] M. Praehofer and H. Spohn, J. Stat. Phys. **115**, 255 (2004).
  - [2] M. Praehofer and H. Spohn, Phys. Rev. Lett. **84**, 4882 (2000), J. Baik and E. M. Rain, J. Stat. Phys. **100**, 523 (2000).
  - [3] M. Kardar, G. Parisi, and Y.-C. Zhang, Phys. Rev. Lett. **56**, 889 (1986).
  - [4] T. Halpin-Healy and Y. Zhang, Phys. Rep. **245**, 218 (1995).
  - [5] D. Forster, D. R. Nelson, and M. J. Stephen, Phys. Rev. A **16**, 732 (1977).
  - [6] M. Kardar, Nucl. Phys. B **290**, 582 (1987).
  - [7] H. van Beijeren, R. Kutner, and H. Spohn, Phys. Rev. Lett. **54**, 2026 (1985).
  - [8] H. K. Janssen and B. Schmittmann, Z. Phys. B **63**, 517 (1986).
  - [9] T. Hwa, Phys. Rev. Lett. **69**, 1552 (1992).
  - [10] K. A. Takeuchi and M. Sano, Phys. Rev. Lett. **104**, 230601 (2010).
  - [11] E. Katzav and M. Schwartz, Physica (Amsterdam) **309A**, 69 (2002).
  - [12] L. Canet, H. Chaté, B. Delamotte, N. Wschebor, Phys. Rev. Lett. **104**, 150601 (2010).
  - [13] K. J. Wiese, J. Stat. Phys. **93**, 143 (1998).
  - [14] E. Frey, U. C. Täuber, and T. Hwa, Phys. Rev. E **53**, 4424 (1996).
  - [15] J.-P. Bouchaud and M. E. Cates, Phys. Rev. E **47**, R1455 (1993).
  - [16] J. P. Doherty, M. A. Moore, J. Kim, and A. J. Bray, Phys. Rev. Lett. **72**, 2041 (1994).
  - [17] F. Colaioni and M. A. Moore, Phys. Rev. Lett. **86**, 3946 (2001).
  - [18] H. C. Fogedby, Phys. Rev. Lett. **94**, 195702 (2005), Phys. Rev. E **73**, 031104 (2006).

- [19] M. Schwartz and S.F. Edwards, Europhys. Lett. **20** 301 (1992); M. Schwartz and S.F. Edwards, Phys. Rev. E **57** 5730 (1998), M. Moshe and E. Katzav, J. Stat. Mech. **P04023** (2008).
- [20] T. Sasamoto, J. Phys. A: Math. Gen. **38**, 549 (2005).
- [21] During the completion of this work, the complete exact solution of the one-dimensional equation for curved initial conditions has become available, see T. Sasamoto and H. Spohn, Phys. Rev. Lett. **104**, 230602 (2010) and references therein.
- [22] P. Calabrese and P. Le Doussal, Phys. Rev. Lett. **106**, 250603 (2011).
- [23] T. Hwa and E. Frey, Phys. Rev. A **44**, R7873 (1991).
- [24] F. Colaioni and M. A. Moore, Phys. Rev. E **65**, 017105 (2001).
- [25] M. Tissier, B. Delamotte, and D. Mouhanna, Phys. Rev. Lett. **84**, 5208 (2000), B. Delamotte, D. Mouhanna, and M. Tissier, Phys. Rev. B **69**, 134413 (2004).
- [26] G. Tarjus and M. Tissier, Phys. Rev. Lett. **93**, 267008 (2004), M. Tissier and G. Tarjus, Phys. Rev. Lett. **96**, 087202 (2006), G. Tarjus and M. Tissier, Phys. Rev. B **78**, 024203 (2008), M. Tissier and G. Tarjus, Phys. Rev. B **78**, 024204 (2008).
- [27] J.-P. Kownacki, and D. Mouhanna, Phys. Rev. E **79**, 040101 (2009); K. Essafi, J.-P. Kownacki, and D. Mouhanna, Phys. Rev. Lett. **106**, 128102 (2011).
- [28] N. Dupuis, Phys. Rev. Lett. **102**, 190401 (2009), Phys. Rev. A **80**, 043627 (2009), A. Rançon and N. Dupuis, Phys. Rev. B **83**, 172501 (2011).
- [29] L. Canet, B. Delamotte, O. Deloubrière, and N. Wschebor, Phys. Rev. Lett. **92**, 195703 (2004), L. Canet, H. Chaté, and B. Delamotte, Phys. Rev. Lett. **92**, 255703 (2004), L. Canet, H. Chaté, B. Delamotte, I. Dornic, and M. A. Muñoz, Phys. Rev. Lett. **95**, 100601 (2005).
- [30] H. K. Janssen, Z. Phys. B **23**, 377 (1976), C. de Dominicis, J. Phys. (Paris) C **1**, 247 (1976).
- [31] J. Berges, N. Tetradis, and C. Wetterich, Phys. Rep. **363**, 223 (2002).
- [32] B. Delamotte, ArXiv: cond-mat/0702365.
- [33] L. Canet, H. Chaté and B. Delamotte, *arXiv:1106.4129*.
- [34] L. Canet, arxiv:cond-mat/0509541.
- [35] V. V. Lebedev and V. S. L'vov, Phys. Rev. E **49**, R959 (1994).
- [36] J.-P. Blaizot, R. Méndez-Galain, and N. Wschebor, Phys. Lett. B **632**, 571 (2006), F. Benitez, J. -P. Blaizot, H. Chaté *et al.*, Phys. Rev. E **80**, 030103 (2009).
- [37] D. Guerra, R. Méndez-Galain, and N. Wschebor, Eur. Phys. J. B **59**:357 (2007).
- [38] L.-H. Tang, B. M. Forrest, and D. E. Wolf, Phys. Rev. A **45**, 7162 (1992), E. Marinari, A. Pagnani, and G. Parisi, J. Phys. A **33**, 8181 (2000).
- [39] C. Castellano, M. Marsili, and L. Pietronero, Phys. Rev. Lett. **80**, 3527 (1998).
- [40] T. Halpin-Healy, Phys. Rev. A, **42**, 711 (1990); M. Lässig and H. Kinzelbach, Phys. Rev. Lett. **78**, 903 (1997); J. K. Bhattacharjee, J. Phys. A **31**, L93 (1998).
- [41] E. Frey and U.C. Täuber, Phys. Rev. E **50**, 1024 (1994).
- [42] C. A. Doty and J. M. Kosterlitz, Phys. Rev. Lett. **69**, 1979 (1992).
- [43] L. Canet, B. Delamotte, D. Mouhanna, and J. Vidal, Phys. Rev. D **67**, 065004 (2003), L. Canet, B. Delamotte, D. Mouhanna, and J. Vidal, Phys. Rev. B **68**, 064421 (2003).
- [44] E. Katzav and M. Schwartz, Phys. Rev. E **69**, 052603 (2004).
- [45] This is done to improve the quality of the fit, otherwise the relative weight of the tail is very small in the fitting procedure.
- [46] The only exception to  $\pm z_0^\pm$  lying the closest to the real axis comes from spurious poles of the rational fraction inside the power law in (69) that are also zeros of the numerator and therefore do not contribute. Those artifacts appear ponctually and do not persist from an order of the fit to the other.